

GIANT MOLECULAR CLOUD EVOLUTIONS IN THE NEARBY SPIRAL GALAXY M33

RIE E. MIURA^{1,2,3}, KOTARO KOHNO^{3,4}, TOMOKA TOSAKI⁵, DANIEL ESPADA¹, NARAE HWANG¹, NARIO KUNO⁶, SACHIKO K. OKUMURA^{1,2,7}, AKIHIKO HIROTA⁶, KAZUYUKI MURAOKA⁸, SACHIKO ONODERA^{6,9}, TETSUHIRO MINAMIDANI¹⁰, SHINYA KOMUGI^{1,11}, KOUCIHIRO NAKANISHI^{1,11,12}, TSUYOSHI SAWADA^{1,11}, HIROYUKI KANEKO^{6,12,13}, AND RYOHEI KAWABE^{6,11}

¹ National Astronomical Observatory of Japan, 2-21-1 Osawa, Mitaka, Tokyo 181-8588, Japan; rie.miura@nao.ac.jp

² Department of Astronomy, The University of Tokyo, Hongo, Bunkyo-ku, Tokyo 133-0033, Japan

³ Institute of Astronomy, School of Science, The University of Tokyo, Osawa, Mitaka, Tokyo 181-0015, Japan

⁴ Research Center for Early Universe, School of Science, The University of Tokyo, Hongo, Bunkyo, Tokyo 113-0033, Japan

⁵ Department of Geoscience, Joetsu University of Education, Yamayashiki-machi, Joetsu, Niigata 943-8512, Japan

⁶ Nobeyama Radio Observatory, Minamimaki, Minamisaku, Nagano 384-1805, Japan

⁷ Department of Mathematical and Physical Sciences, Faculty of Science, Japan Woman's University, Mejirodai 2-8-1, Bunkyo, Tokyo 112-8681, Japan

⁸ Department of Physical Science, Osaka Prefecture University, Gakuen 1-1, Sakai, Osaka 599-8531, Japan

⁹ Department of Physics, Meisei University, Hino, Tokyo 191-8506, Japan

¹⁰ Department of Physics, Faculty of Science, Hokkaido University, N10W8, Kita-ku, Sapporo 060-0810, Japan

¹¹ Joint ALMA Observatory, Alonso de Cordova 3107, Vitacura 763-0355, Santiago de Chile

¹² Department of Astronomical Science, The Graduate University for Advanced Studies (Sokendai), 2-21-1 Osawa, Mitaka, Tokyo 181-0015, Japan

¹³ Graduate School of Pure and Applied Sciences, Institute of Physics, University of Tsukuba, 1-1-1 Tennodai, Tsukuba, Ibaraki 305-8571, Japan

Received 2012 May 14; accepted 2012 October 11; published 2012 November 20

ABSTRACT

We present a giant molecular cloud (GMC) catalog of M33, containing 71 GMCs in total, based on wide-field and high-sensitivity CO($J = 3-2$) observations with a spatial resolution of 100 pc using the ASTE 10 m telescope. Employing archival optical data, we identify 75 young stellar groups (YSGs) from the excess of the surface stellar density, and estimate their ages by comparing with stellar evolution models. A spatial comparison among the GMCs, YSGs, and H II regions enable us to classify GMCs into four categories: Type A, showing no sign of massive star formation (SF); Type B, being associated only with H II regions; Type C, with both H II regions and <10 Myr old YSGs; and Type D, with both H II regions and 10–30 Myr YSGs. Out of 65 GMCs (discarding those at the edges of the observed fields), 1 (1%), 13 (20%), 29 (45%), and 22 (34%) are Types A, B, C, and D, respectively. We interpret these categories as stages in a GMC evolutionary sequence. Assuming that the timescale for each evolutionary stage is proportional to the number of GMCs, the lifetime of a GMC with a mass $>10^5 M_\odot$ is estimated to be 20–40 Myr. In addition, we find that the dense gas fraction as traced by the CO($J = 3-2$)/CO($J = 1-0$) ratio is enhanced around SF regions. This confirms a scenario where dense gas is preferentially formed around previously generated stars, and will be the fuel for the next stellar generation. In this way, massive SF gradually propagates in a GMC until gas is exhausted.

Key words: galaxies: individual (M33) – ISM: clouds – ISM: molecules – submillimeter: ISM

Online-only material: color figures, figure set

1. INTRODUCTION

Observations in our Galaxy and in the Local Group of Galaxies (LGGs) have revealed that giant molecular clouds (GMCs) have masses of about 10^4 – $10^7 M_\odot$ and sizes of 50 to several hundred parsecs (e.g., Blitz 1993; Fukui & Kawamura 2010), which are often found associated with H II regions and OB associations (Massey 2003), tracers of massive star formation (SF). Massive stars, which are commonly found clustered in OB associations (Lada & Lada 2003), are short-lived (less than a few 10 Myr), and thus spend most of their lifetime within the cluster in which they were formed. This suggests that GMCs are the principal sites of massive SF. However, how SF occurs in a GMC, the so-called GMC evolution, has remained poorly understood because it has been difficult to perform molecular gas observations with a combination of high resolution, sensitivity, and wide field to enable studies of a sufficiently large sample of GMCs. Such studies in LGGs have the potential to reveal the density distribution and kinematics at GMC scales, as well as its relation to ongoing SF.

Several studies focusing on GMC evolution in the Large Magellanic Clouds (LMCs) have been performed (e.g., Fukui et al. 1999; Mizuno et al. 2001; Yamaguchi et al. 2001;

Kawamura et al. 2009). The GMCs in the LMC are classified into three types according to their associated massive SF activities: Type I showing no signature of massive SF, Type II being associated with relatively small H II regions, and Type III with both H II regions and young (less than 10 Myr old) stellar clusters (Yamaguchi et al. 2001; Kawamura et al. 2009). While in general the positions of young clusters are correlated with GMCs, the clusters older than 10 Myr have a weaker or no correlation with the GMCs (Kawamura et al. 2009). This classification was interpreted to be a template for the GMC evolutionary stages, and the typical lifetime of GMCs with masses larger than $5 \times 10^4 M_\odot$ is estimated to be 20–30 Myr (Blitz et al. 2007; Kawamura et al. 2009). Analyses of the kinetic temperature and density of several GMCs in LMC shows that they increase generally as the GMCs evolve (Minamidani et al. 2008; Pineda et al. 2008; Mizuno et al. 2010; Minamidani et al. 2011). This confirms that the denser and warmer molecular gas is directly linked to SF activities. Because these studies are only limited to several specific GMCs in one irregular galaxy, it is still necessary to investigate the properties of GMCs in the different environments present in other galaxies, in order to complete our current knowledge of templates for GMC evolution.

M33 is one of the best laboratories for studying GMC evolutions under different environments due to its proximity (distance of 840 kpc; Freedman et al. 2001) and favorable inclination ($i = 51^\circ$; Corbelli & Salucci 2000), as well as the existence of spiral structure and massive SF regions. M33 is the second-closest spiral galaxy after M31, but M33 is less inclined, which is ideal for resolving gas components or individual stars with little contamination along the line of sight. Also, studying GMCs over a disk galaxy enables us to compare all GMCs at the same distance, unlike in our Galaxy.

Surveys of $^{12}\text{CO}(J = 1-0)$ and $^{12}\text{CO}(J = 2-1)$ emission in M33 to investigate the relation between molecular gas and massive SF have been conducted by several authors (Engargiola et al. 2003; Heyer et al. 2004; Rosolowsky et al. 2007; Gratier et al. 2010; Tosaki et al. 2011; Gratier et al. 2012). Engargiola et al. (2003) have found that more than two-thirds of the GMCs in M33 are associated with H II regions within 50 pc, which is similar to the proportion in LMC (Yamaguchi et al. 2001; Kawamura et al. 2009). On the other hand, the correlation between the molecular gas surface densities traced by $\text{CO}(J = 1-0)$ emission and that of star formation rate (SFR), the so-called Kennicutt–Schmidt law (hereafter K-S law; Schmidt 1959; Kennicutt 1989) in a pixel-to-pixel analysis is found to be weaker at 80 pc resolutions (Onodera et al. 2010) than at lower resolutions (200 pc; Heyer et al. 2004). This suggests that the GMCs traced by $\text{CO}(J = 1-0)$ are well correlated with the massive SF sites, but their peaks are offset from each other.

Recently, the K-S law using $\text{CO}(J = 3-2)$ in M33 has shown a tight correlation at 100 pc resolution, unlike $\text{CO}(J = 1-0)$ (Onodera et al. 2013). In fact, with higher resolution data, Tosaki et al. (2007) have found that the $\text{CO}(J = 3-2)$ emission is spatially better correlated to massive SF sites than $\text{CO}(J = 1-0)$ in the most luminous giant H II region (GHR) in M33, NGC 604. This supports that the dense and warm gas traced by $\text{CO}(J = 3-2)$ is more closely linked to the SF sites, as previously argued for four Virgo galaxies in Wilson et al. (2009). These results are interpreted as higher kinetic temperatures and densities in GMCs found close to GHRs, in agreement with large velocity gradient analysis with multi- J CO transition data by Wilson et al. (1997) and Muraoka et al. (2012).

As part of the Nobeyama Radio Observatory (NRO) M33 All-disk Survey of Giant Molecular Clouds project (Tosaki et al. 2011), here we present a catalog of M33 GMCs using new $\text{CO}(J = 3-2)$ maps with $25''$ (corresponding to 100 pc) resolution. In order to investigate the relation of the GMCs with massive SF, we also present a “young stellar group (YSG)” catalog. In this work, YSGs can be clusters (typical sizes of 15 pc), OB associations (typical sizes of $\sim 15\text{--}100$ pc), and star complexes (sizes of a few hundred parsecs) (e.g., Battinelli et al. 1996; Ivanov 2005). There are a number of catalogs for clusters, OB associations, and star complexes in M33 published so far (e.g., Sarajedini & Mancone 2007, hereafter SM; Park & Lee 2007; San Roman et al. 2010; Humphreys & Sandage 1980; Ivanov 2005). However, the number of star clusters whose ages have been estimated is limited, and the methods for deriving the ages are not homogenous (SM and references therein; Park et al. 2009, hereafter PPL; San Roman et al. 2009, hereafter SSGH). We also aim to estimate their ages in a homogeneous manner using the stellar photometry catalog provided by Massey et al. (2006).

The outline of this paper is as follows. The observations and data reduction are summarized in Section 2. In Section 3 we explain the general procedure for identifying GMCs, as well as

the identification of YSGs and the estimation of their ages. We classify GMCs as a function of the age of YSGs associated with them. We also quantify the SF activities and dense gas fractions in the GMCs using the extinction-corrected $\text{H}\alpha$ data and the $\text{CO}(J = 3-2)/\text{CO}(J = 1-0)$ line ratio, $R_{3-2/1-0}$, and then show the variety of physical states of the identified GMCs. In Section 4, we discuss the relationship between the properties of these clouds and their evolutionary stages. Finally, we interpret our results in the context of a continuous SF in GMCs. The summary of this paper is provided in Section 5.

2. OBSERVATIONS AND DATA REDUCTION

We describe the data that is used throughout this paper, including the $\text{CO}(J = 3-2)$ data to identify the GMCs, the $\text{CO}(J = 1-0)$ data to derive $R_{3-2/1-0}$, and the optical and infrared data to identify the YSG and H II regions in M33.

2.1. ASTE $\text{CO}(J = 3-2)$ Data

We chose eight regions covering the northern and southern spiral arms as well as the galaxy center, where the $\text{CO}(J = 1-0)$ emission is prominent (Tosaki et al. 2011). The $\text{CO}(J = 3-2)$ (rest frequency: 345.796 GHz) mapping observations were performed between 2011 June and November, using the Atacama Submillimeter Telescope Experiment (ASTE; Ezawa et al. 2004, 2008; Kohno 2005) 10 m dish equipped with the 345 GHz side band separating (2SB) SIS receiver CATS345 (CArtridge-Type Sideband-separating receiver for ASTE 345-GHz band; Inoue et al. 2008). An XF-Type digital spectrometer MAC (Sorai et al. 2000) was used to cover a velocity width of 445 km s^{-1} with a velocity resolution of 2.5 km s^{-1} at 345 GHz. The on-the-fly (OTF) mapping technique (Mangum et al. 2007), based on scanning smoothly and rapidly along one direction across a rectangular map, was employed to obtain the $\text{CO}(J = 3-2)$ data. The observed area covers in total about 80% of the $\text{CO}(J = 1-0)$ based molecular gas mass in Tosaki et al. (2011).

The observations and the data calibration were performed for each region as follows. The half-power beam width (HPBW) of the ASTE 10 m telescope is $22''$ at 345 GHz. The chopper-wheel technique was employed to calibrate the antenna temperature T_A^* and the final data have been converted into units of main-beam brightness temperature ($T_{\text{mb}} \equiv T_A^*/\eta_{\text{mb}}$), where η_{mb} is the main-beam efficiency, measured to be 0.6 ± 0.1 using the standard source Orion KL at $(\alpha_{J2000}, \delta_{J2000}) = (05^{\text{h}}35^{\text{m}}14\overset{\text{s}}{.}5, 05^{\circ}22'29\overset{\text{s}}{.}6)$. Hereafter, all the CO intensity measurements are specified in T_{mb} . The typical system temperatures in a single side band were usually less than 200 K. The absolute pointing accuracy was verified by observing the $\text{CO}(J = 3-2)$ emission of o-Cet at 1–1.5 hr intervals, and it was kept better than $4''$ rms. The absolute intensity stability was also monitored using o-Cet during the different observing runs and was found to be stable within $\sim 16\%$.

The data reduction was carried out with the Nobeyama OTF Software Tools for Analysis and Reduction package (NOSTAR; Sawada et al. 2008). The “scanning noise” was removed by combining scans using the PLAIT algorithm as described by Emerson & Graeve (1988). The data have been convolved with a Bessel–Gauss function in the spectral domain to create the data cube. The final grid spacing is $8''.0$ and the angular resolution is $25''$. The final data cubes for the eight regions are characterized by an rms noise of $\sigma_{\text{ch}} = 16\text{--}32 \text{ mK}$ in a velocity resolution of 2.5 km s^{-1} , achieved after 87 hr of total integration. We briefly summarize in Table 1 the observational and data reduction

Table 1
Properties of the ASTE CO($J = 3-2$) Observations

Region No.	Map Center R.A., Decl. (J2000.0)	Area (arcsec, arcsec)	Int. Time (hr)	σ_{ch} (mK)
(1)	(2)	(3)	(4)	(5)
1	1 ^h 33 ^m 44 ^s .4, 30°38'12".2	310 × 335	22.5	16
2	1 ^h 34 ^m 08 ^s .5, 30°37'36".4	263 × 240	8.7	19
3	1 ^h 34 ^m 12 ^s .8, 30°34'28".9	150 × 135	1.3	25
4	1 ^h 33 ^m 38 ^s .5, 30°32'45".0	200 × 440	21.8	18
5	1 ^h 33 ^m 35 ^s .0, 30°41'48".0	120 × 120	1.9	32
6	1 ^h 34 ^m 05 ^s .5, 30°48'02".9	250 × 250	12.8	19
7	1 ^h 34 ^m 33 ^s .2, 30°47'06".0	210 × 210	10.5	25
8	1 ^h 34 ^m 38 ^s .5, 30°40'55".0	180 × 150	7.0	18

Notes. Column 1: No. of the eight observed regions in order of increasing galaxy radius. Column 2: central position of each region. Column 3: size of the observed region. Column 4: integration time for each region. Column 5: rms for a 2.5 km s⁻¹ channel, measured in an emission-free region.

parameters for the eight observed regions, including their central positions, sizes, integration times, and rms for a 2.5 km s⁻¹ channel.

Figure 1 shows the obtained integrated intensity map over the velocity range $V_{\text{LSR}} = -274$ km s⁻¹ to -94 km s⁻¹, where emission is $>2 \sigma_{\text{ch}}$, overlaid on the H α image (Section 2.3). The rms noise level of the integrated intensity map (σ_{mon}) is 0.38 K km s⁻¹ on average. The noise level of the CO($J = 3-2$) integrated intensity map is calculated using $\sigma_{\text{mon}} \equiv \sigma_{\text{ch}} \sqrt{N \delta v}$, where N is the number of integrated channels and δv is the velocity resolution of a channel (2.5 km s⁻¹). The observed fields cover the molecular disk up to the galactic radius of ~ 5 kpc. Note that we also present CO-integrated intensity maps for each individual GMC in Section 3.1.1 and the Appendix.

2.2. NRO CO($J = 1-0$) Data

The CO($J = 1-0$) emission was observed in a $31' \times 36'$ area (corresponding to 7.6 kpc \times 8.8 kpc) toward the disk of M33 using the NRO 45 m telescope (Tosaki et al. 2011). The data reduction was also carried out with the NOSTAR reduction package. The angular resolution of the final map was 19''.3 and the grid spacing 7''.5. Further processing was done with MIRIAD (Sault et al. 1995) in a manner similar to the CO($J = 3-2$) map. We have convolved the CO($J = 1-0$) map to a common angular resolution of 25'' and re-gridded it to 8''.0 pixel⁻¹. The convolved map had an rms noise of 87 mK for the velocity resolution of 2.5 km s⁻¹. We have also created CO($J = 1-0$) integrated intensity maps for each GMC (see the Appendix), integrating over the same velocity range as used for the individual CO($J = 3-2$) integrated intensity maps.

2.3. Optical and Infrared Data

We have used the photometric optical data set from the *UBVI* ground-based survey of local star-forming galaxies with the Kitt Peak National Observatory 4 m telescope presented in Massey et al. (2006), and available on their ftp site.¹⁴ It contains a total of 146,622 stars in a field of 0.8 deg² centered on M33, which fully covers the regions that were observed in CO($J = 3-2$) and CO($J = 1-0$). The photometry in *BVI* bands is less than 1% above 21.1 mag and even less than 10% at about 23 mag. Refer

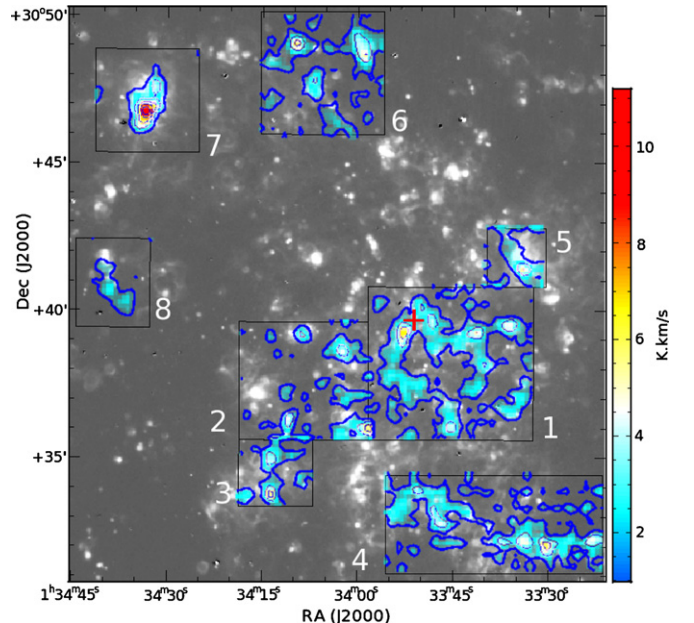


Figure 1. CO($J = 3-2$) integrated intensity map with 25'' resolution (~ 100 pc), overlaid on the H α image. The color range spans from 1 to 11 K km s⁻¹ and contour levels are 1, 3, 5, 7, and 9 K km s⁻¹. The rectangular boxes indicate the eight observed regions in CO($J = 3-2$), and the number identifies each region in Table 1. The cross symbol in Box 1 represents the galaxy center.

to Massey et al. (2006) for further details about the observation, data reduction, and photometric analysis.

We have also compiled available H II region catalogs (Courtes et al. 1987; Wyder et al. 1997; Hodge et al. 1999). The H α image from Hoopes & Walterbos (2000) is used to check the accuracy of the positions and extents of the M33 individual H II regions in these catalogs. Refer to Hoopes & Walterbos (2000) for more details on the observations and reduction process.

Finally, we have used the 24 μ m *Spitzer* data presented in Onodera et al. (2010) to correct the extinction in the H α emission. The final combined mosaic image is approximately 1.1 \times 1.2 deg², and both the point-spread function FWHM and grid sizes are set to 5''.7. For more details on the reduction process, refer to Onodera et al. (2010 and references therein). Note that Onodera et al. (2010) have performed a pixel-by-pixel analysis and have not applied a local background subtraction to create the extinction-corrected data by combining the H α image and the 24 μ m data. The lack of background subtraction may cause a systematic shift in the extinction-corrected H α luminosity (e.g., Kennicutt et al. 2009). In this paper, instead, we present a new approach in which the H α and 24 μ m luminosities are measured with circular apertures of several 100 pc radius and with local background subtraction applied (see Section 3.3). We use the catalog of 24 μ m sources in Verley et al. (2007), which is the only reference listing 24 μ m sources to date, for the sake of comparing the positions of H II regions.

3. RESULTS

3.1. The CO($J = 3-2$) GMC Catalog

The GMC catalog is obtained from our CO($J = 3-2$) data using the CPROPS package described in Rosolowsky & Leroy (2006). Briefly, we search for compact emission in adjacent pairs of channels with $T_{\text{mb}} > 4 \sigma_{\text{rms}}$, the so-called *cores*, and then for emission with $T_{\text{mb}} > 2 \sigma_{\text{rms}}$ connected to such cores. CPROPS attempts to account for the amount of flux below the $2 \sigma_{\text{rms}}$ cutoff

¹⁴ <http://ftp.lowell.edu/pub/massey/lgsurvey/>

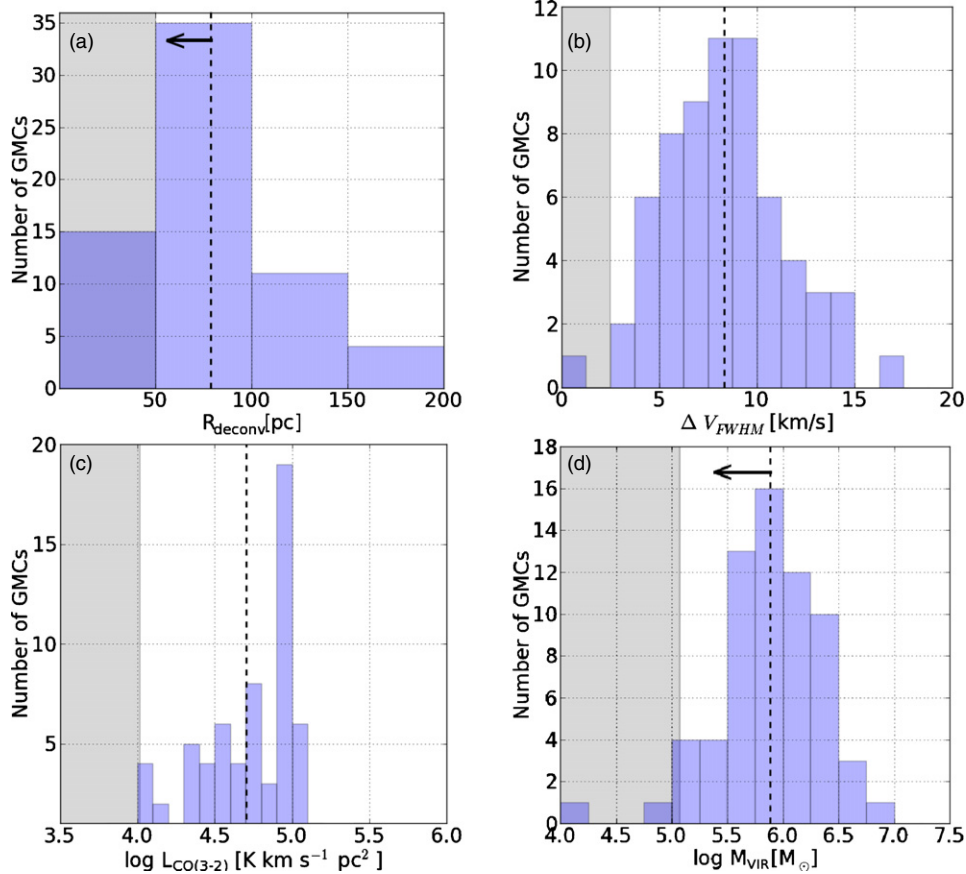


Figure 2. Histograms of physical properties of GMCs as traced by CO($J = 3-2$): (a) deconvolved radius (R_{deconv}), (b) FWHM line width (ΔV_{FWHM}), (c) luminosity ($L'_{\text{CO}(3-2)}$), and (d) virial mass (M_{vir}). The shaded areas indicate the detection limit. The dashed lines represent the average values: $R_{\text{deconv}} \lesssim 73$ pc, $\Delta V_{\text{FWHM}} \simeq 8.3$ km s $^{-1}$, $L'_{\text{CO}(3-2)} \simeq 5.1 \times 10^4$ K km s $^{-1}$ pc 2 , and $M_{\text{vir}} \lesssim 7.6 \times 10^5 M_{\odot}$.

(A color version of this figure is available in the online journal.)

by linearly extrapolating the emission profile to the 0 K km s $^{-1}$ intensity level. Finally, the emission identified with CPROPS must have a minimum velocity width of 2 channels (5 km s $^{-1}$) with a minimum peak of $T_{\text{mb}} > 4\sigma_{\text{rms}}$, and an equivalent size of at least the spatial resolution of 25'' (~ 100 pc). Therefore, GMCs with a narrower velocity width than 2.5 km s $^{-1}$ (if any) will not be identified by this analysis.

As a result, we have identified a total of 71 GMCs, whose properties are summarized in Table 2. The columns indicate the cloud ID, the cloud position (R.A., decl.), the velocity, the peak intensity, the FWHM of the velocity width (ΔV_{FWHM}), the major/minor axes and orientation of the GMCs, the CO($J = 3-2$) luminosity ($L'_{\text{CO}(3-2)}$), virial mass (M_{vir}), and cross identifications with the CO($J = 1-0$) and CO($J = 2-1$) GMC catalogs of previous papers (Rosolowsky et al. 2007; Gratier et al. 2012). The cloud position and velocity are derived from an intensity-weighted mean over all the pixels of a GMC. The major/minor diameters (A_{maj} , A_{min}) without beam deconvolution are also indicated. The virial mass, calculated under the assumption that each cloud is spherical and can be parameterized by a density profile $\rho \propto r^{-\beta}$, is given by $M_{\text{vir}} = 189 \Delta V_{\text{FWHM}}^2 R_{\text{deconv}} M_{\odot}$ (Solomon et al. 1987), where R_{deconv} is the deconvolved radius given by deconvolving the beam size (θ_{beam}) from the GMC size, i.e., $R_{\text{deconv}} = \sqrt{[A_{\text{maj}}^2 - \theta_{\text{beam}}^2]^{1/2} [A_{\text{min}}^2 - \theta_{\text{beam}}^2]^{1/2}}$. Note that the virial masses of 27 GMCs are not shown because their minor diameters are smaller than the beam size.

Among the 71 GMCs in our catalog, only one GMC (GMC-50) is a new identification. The 70 GMCs have

been previously identified in lower- J CO transition catalogs (Rosolowsky et al. 2007; Gratier et al. 2012). GMC-50 is located outside of the observed field in Gratier et al. (2012) and has a marginal detection in the CO($J = 1-0$) integrated intensity map in Rosolowsky et al. (2007), but was not identified in their catalog. A total of 10 GMCs in our catalog are composed of more than two smaller GMCs in previous catalogs, due to their higher resolution data (~ 50 pc; Rosolowsky et al. 2007; Gratier et al. 2012). On the other hand, a few single GMCs in the Rosolowsky et al.'s (2007) catalog appear to be composed of more than two GMCs in our catalog. This is because of our 8–15 times better sensitivity data, since decomposition of neighboring clouds is done based on peak differences exceeding $2\sigma_{\text{rms}}$ (Rosolowsky & Leroy 2006). The ID numbers in these cases are marked with an asterisk in Table 2. Since six GMCs (GMC-18, GMC-28, GMC-47, GMC-51, GMC-58, and GMC-71) are at the edge of the observed fields and their extents are uncertain, they are not included in further analysis and discussion.

Histograms of the physical properties of 65 GMCs are presented in Figure 2. The ΔV_{FWHM} , R_{deconv} , $L'_{\text{CO}(3-2)}$, and M_{vir} are in the range of 1.2–17.3 km s $^{-1}$, 12–157 pc, $(0.8-25.8) \times 10^4$ K km s $^{-1}$ pc 2 , and $(0.2-89.2) \times 10^5 M_{\odot}$, respectively. A lower limit for the virial mass is $1.2 \times 10^5 M_{\odot}$, assuming an effective radius of ~ 50 pc and $\Delta V_{\text{FWHM}} = 2.5$ km s $^{-1}$, which are close to the instrumental limits. Average values are $\Delta V_{\text{FWHM}} \simeq 8.3$ km s $^{-1}$, $R_{\text{deconv}} \lesssim 73$ pc, $L'_{\text{CO}(3-2)} \sim 5.1 \times 10^4$ K km s $^{-1}$ pc 2 , and $M_{\text{vir}} \lesssim 7.7 \times 10^5 M_{\odot}$. Note that we have used the non-deconvolved radius for the GMCs whose minor axes were

Table 2
Properties of the CO ($J = 3-2$) Emission Components

GMC ID	R.A., Decl. (J2000.0)	V_{LSR} (km s $^{-1}$)	T_{mb} (K)	ΔV_{FWHM} (km s $^{-1}$)	$A_{\text{maj}} \times A_{\text{min}}$ (pc \times pc)	$L'_{\text{CO}(3-2)}$ (10^4 K km s $^{-1}$ pc 2)	M_{vir} ($10^5 M_{\odot}$)	$R_{3-2/1-0}$	Cross ID
(1)	(2)	(3)	(4)	(5)	(6)	(7)	(8)	(9)	(10)
1	1 $^{\text{h}}34^{\text{m}}33^{\text{s}}.2$, 30°46'52"5	-243	0.84	13.8 ± 2.8	$72 \times 59(42^{\circ})$	25.8 ± 1.6	24.4 ± 1.6	0.89 ± 0.46	R07-124, G11-215
2	1 $^{\text{h}}33^{\text{m}}58^{\text{s}}.7$, 30°48'44"5	-245	0.69	5.6 ± 2.6	$54 \times 46(91^{\circ})$	8.3 ± 6.1	...	0.52 ± 0.09	R07-86 ^a , G11-242
3	1 $^{\text{h}}34^{\text{m}}13^{\text{s}}.8$, 30°33'43"9	-157	0.62	9.5 ± 2.4	$51 \times 49(135^{\circ})$	8.5 ± 1.4	2.0 ± 0.3	0.52 ± 0.12	R07-105
4	1 $^{\text{h}}34^{\text{m}}10^{\text{s}}.8$, 30°36'15"2	-160	0.60	6.6 ± 1.1	$65 \times 42(83^{\circ})$	5.6 ± 0.5	...	0.45 ± 0.11	R07-76
5	1 $^{\text{h}}33^{\text{m}}52^{\text{s}}.5$, 30°39'19"8	-168	0.59	10.0 ± 1.7	$59 \times 50(29^{\circ})$	9.6 ± 0.7	4.6 ± 0.3	0.52 ± 0.15	R07-1, G11-108
6	1 $^{\text{h}}33^{\text{m}}36^{\text{s}}.2$, 30°39'28"5	-168	0.55	7.8 ± 1.3	$89 \times 47(180^{\circ})$	9.4 ± 1.0	...	0.37 ± 0.07	R07-34, G11-105, 108
7	1 $^{\text{h}}33^{\text{m}}33^{\text{s}}.7$, 30°41'25"6	-185	0.53	9.9 ± 2.4	$60 \times 45(150^{\circ})$	8.3 ± 0.9	...	0.84 ± 0.36	R07-49
8	1 $^{\text{h}}34^{\text{m}}09^{\text{s}}.4$, 30°49'07"9	-249	0.50	10.4 ± 1.8	$55 \times 47(137^{\circ})$	9.4 ± 0.9	...	0.26 ± 0.03	R07-91, G11-245
9	1 $^{\text{h}}33^{\text{m}}35^{\text{s}}.5$, 30°36'29"2	-135	0.48	8.5 ± 4.3	$63 \times 54(5^{\circ})$	9.6 ± 6.8	6.7 ± 4.8	0.59 ± 0.08	R07-37, G11-87
10	1 $^{\text{h}}33^{\text{m}}45^{\text{s}}.1$, 30°36'02"1	-139	0.47	9.2 ± 3.1	$65 \times 54(107^{\circ})$	9.4 ± 4.0	7.9 ± 3.3	0.56 ± 0.11	R07-28, G11-65
11	1 $^{\text{h}}33^{\text{m}}49^{\text{s}}.6$, 30°33'55"0	-134	0.46	5.5 ± 1.1	$125 \times 49(161^{\circ})$	6.1 ± 0.6	...	0.40 ± 0.06	R07-47, G11-29, 30
12	1 $^{\text{h}}34^{\text{m}}08^{\text{s}}.8$, 30°39'12"4	-194	0.46	6.7 ± 1.3	$52 \times 49(161^{\circ})$	5.7 ± 0.6	1.1 ± 0.1	0.34 ± 0.07	R07-46, G11-171
13	1 $^{\text{h}}33^{\text{m}}29^{\text{s}}.9$, 30°31'59"7	-133	0.46	9.2 ± 2.1	$62 \times 57(174^{\circ})$	8.8 ± 1.8	8.6 ± 1.7	0.49 ± 0.08	R07-82, G11-35, 43
14	1 $^{\text{h}}34^{\text{m}}06^{\text{s}}.8$, 30°47'43"1	-255	0.45	8.6 ± 1.1	$88 \times 55(87^{\circ})$	9.5 ± 0.8	9.7 ± 0.8	0.38 ± 0.08	R07-81, G11-256
15	1 $^{\text{h}}33^{\text{m}}41^{\text{s}}.0$, 30°39'11"5	-165	0.43	7.7 ± 3.4	$58 \times 47(6^{\circ})$	5.7 ± 3.6	...	0.34 ± 0.04	R07-22, G11-103
16	1 $^{\text{h}}33^{\text{m}}59^{\text{s}}.5$, 30°49'11"6	-251	0.42	13.2 ± 14.4	$119 \times 62(96^{\circ})$	12.1 ± 27.5	35.2 ± 80.0	0.55 ± 0.09	R07-86 ^a , G11-251
17	1 $^{\text{h}}34^{\text{m}}02^{\text{s}}.5$, 30°39'08"5	-201	0.41	9.2 ± 1.9	$63 \times 43(81^{\circ})$	4.9 ± 0.6	...	0.41 ± 0.07	R07-29, G11-174
18 ^b	1 $^{\text{h}}33^{\text{m}}59^{\text{s}}.4$, 30°36'01"2	-152	0.40	7.0 ± 2.2	$63 \times 38(109^{\circ})$	4.9 ± 2.1	...	0.72 ± 0.20	R07-41
19	1 $^{\text{h}}33^{\text{m}}34^{\text{s}}.7$, 30°37'00"7	-136	0.39	5.4 ± 6.9	$76 \times 99(99^{\circ})$	4.3 ± 5.8	6.4 ± 8.7	0.50 ± 0.18	R07-38, G11-88
20	1 $^{\text{h}}34^{\text{m}}02^{\text{s}}.5$, 30°38'37"6	-185	0.39	10.0 ± 1.6	$84 \times 46(172^{\circ})$	8.3 ± 0.7	...	0.40 ± 0.07	R07-31, G11-170
21	1 $^{\text{h}}33^{\text{m}}55^{\text{s}}.0$, 30°37'41"9	-167	0.37	9.0 ± 2.0	$70 \times 66(68^{\circ})$	7.0 ± 1.4	11.8 ± 2.3	0.39 ± 0.07	R07-17, G11-104
22	1 $^{\text{h}}34^{\text{m}}15^{\text{s}}.5$, 30°39'11"5	-191	0.37	8.9 ± 0.9	$134 \times 72(168^{\circ})$	6.1 ± 0.4	20.0 ± 1.2	0.24 ± 0.03	R07-66, 77, G11-182
23	1 $^{\text{h}}33^{\text{m}}45^{\text{s}}.7$, 30°36'50"6	-144	0.36	8.3 ± 4.7	$124 \times 72(146^{\circ})$	10.8 ± 7.7	16.6 ± 11.9	0.44 ± 0.07	R07-20, G11-61, 62, 66
24	1 $^{\text{h}}33^{\text{m}}47^{\text{s}}.3$, 30°32'52"4	-118	0.35	12.5 ± 2.0	$105 \times 54(114^{\circ})$	11.0 ± 1.6	22.1 ± 3.2	0.59 ± 0.15	R07-61, G11-23
25	1 $^{\text{h}}34^{\text{m}}01^{\text{s}}.5$, 30°36'39"6	-154	0.34	4.9 ± 2.1	$77 \times 44(114^{\circ})$	3.3 ± 1.8	...	0.41 ± 0.04	R07-42
26	1 $^{\text{h}}34^{\text{m}}13^{\text{s}}.8$, 30°34'47"6	-171	0.34	13.0 ± 4.7	$136 \times 50(77^{\circ})$	12.5 ± 3.8	17.5 ± 5.4	0.59 ± 0.13	R07-99
27	1 $^{\text{h}}34^{\text{m}}34^{\text{s}}.5$, 30°46'21"5	-222	0.33	5.8 ± 2.9	$56 \times 39(92^{\circ})$	3.1 ± 1.9	...	0.55 ± 0.17	R07-126, G11-209
28 ^b	1 $^{\text{h}}33^{\text{m}}56^{\text{s}}.7$, 30°40'10"0	-193	0.32	8.9 ± 1.3	$67 \times 53(47^{\circ})$	4.7 ± 0.6	7.4 ± 1.0	0.34 ± 0.06	R07-7, G11-175
29	1 $^{\text{h}}33^{\text{m}}49^{\text{s}}.7$, 30°40'03"3	-193	0.32	12.3 ± 1.8	$76 \times 66(108^{\circ})$	6.3 ± 0.8	23.9 ± 3.0	0.38 ± 0.07	R07-2, G11-114
30	1 $^{\text{h}}33^{\text{m}}33^{\text{s}}.4$, 30°32'16"9	-130	0.32	14.3 ± 4.6	$89 \times 50(34^{\circ})$	8.9 ± 3.6	18.6 ± 7.6	0.58 ± 0.11	R07-73, G11-42
31	1 $^{\text{h}}33^{\text{m}}47^{\text{s}}.1$, 30°38'46"4	-157	0.31	10.8 ± 3.0	$167 \times 63(23^{\circ})$	11.7 ± 3.9	28.8 ± 9.7	0.59 ± 0.08	R07-4, G11-99, 100
32	1 $^{\text{h}}33^{\text{m}}50^{\text{s}}.6$, 30°37'18"2	-147	0.31	10.8 ± 3.8	$117 \times 77(63^{\circ})$	9.8 ± 3.9	28.7 ± 11.4	0.55 ± 0.10	R07-13, G11-91, 92
33	1 $^{\text{h}}34^{\text{m}}32^{\text{s}}.0$, 30°47'38"9	-248	0.30	10.8 ± 5.1	$50 \times 50(77^{\circ})$	11.0 ± 5.7	3.9 ± 2.0	0.79 ± 0.22	R07-123, G11-217
35	1 $^{\text{h}}34^{\text{m}}39^{\text{s}}.1$, 30°40'38"9	-202	0.29	7.7 ± 1.3	$142 \times 79(137^{\circ})$	9.3 ± 1.2	17.0 ± 2.1	0.28 ± 0.04	R07-136 ^a
36	1 $^{\text{h}}34^{\text{m}}03^{\text{s}}.2$, 30°46'34"0	-245	0.29	11.8 ± 2.4	$127 \times 86(136^{\circ})$	8.4 ± 1.1	39.3 ± 5.4	0.32 ± 0.04	R07-62, 64, G11-240, 244
37	1 $^{\text{h}}33^{\text{m}}42^{\text{s}}.9$, 30°33'10"9	-119	0.28	6.4 ± 1.2	$68 \times 55(98^{\circ})$	4.8 ± 0.6	4.4 ± 0.6	0.40 ± 0.08	R07-50, G11-25
38	1 $^{\text{h}}33^{\text{m}}40^{\text{s}}.7$, 30°37'34"1	-145	0.28	17.3 ± 3.1	$189 \times 70(49^{\circ})$	14.3 ± 2.5	88.9 ± 15.7	0.40 ± 0.05	R07-16, 27, G11-68, 69, 70
39	1 $^{\text{h}}33^{\text{m}}33^{\text{s}}.2$, 30°31'58"9	-113	0.28	5.8 ± 2.1	$77 \times 46(171^{\circ})$	3.6 ± 1.4	...	0.46 ± 0.14	R07-75, G11-36
40	1 $^{\text{h}}33^{\text{m}}37^{\text{s}}.6$, 30°32'13"8	-122	0.27	9.9 ± 5.2	$116 \times 58(134^{\circ})$	8.2 ± 5.6	17.5 ± 12.1	0.38 ± 0.05	R07-67, 71, G11-37, 39
41	1 $^{\text{h}}33^{\text{m}}52^{\text{s}}.9$, 30°38'59"5	-150	0.27	7.2 ± 1.6	$59 \times 42(149^{\circ})$	3.0 ± 0.7	...	0.51 ± 0.12	G11-95
42	1 $^{\text{h}}33^{\text{m}}48^{\text{s}}.1$, 30°39'31"5	-168	0.25	9.2 ± 4.8	$70 \times 62(157^{\circ})$	6.9 ± 2.9	11.3 ± 4.6	0.62 ± 0.12	R07-3, G11-107
43	1 $^{\text{h}}33^{\text{m}}53^{\text{s}}.2$, 30°33'10"4	-129	0.24	14.0 ± 3.1	$90 \times 74(86^{\circ})$	9.4 ± 1.6	39.2 ± 6.8	0.39 ± 0.07	R07-60
44	1 $^{\text{h}}33^{\text{m}}52^{\text{s}}.7$, 30°37'11"1	-151	0.24	6.7 ± 5.2	$94 \times 47(94^{\circ})$	7.7 ± 4.3	...	0.41 ± 0.05	R07-19 ^a , G11-94
45	1 $^{\text{h}}33^{\text{m}}52^{\text{s}}.8$, 30°37'41"7	-157	0.24	6.0 ± 4.6	$78 \times 56(84^{\circ})$	3.6 ± 2.3	4.5 ± 2.9	0.47 ± 0.07	R07-19 ^a , G11-98
46	1 $^{\text{h}}33^{\text{m}}42^{\text{s}}.6$, 30°40'10"9	-183	0.24	6.3 ± 2.6	$58 \times 42(9^{\circ})$	2.3 ± 0.8	...	0.40 ± 0.04	G11-112
47 ^b	1 $^{\text{h}}34^{\text{m}}02^{\text{s}}.5$, 30°35'51"8	-150	0.23	5.5 ± 3.5	$81 \times 56(180^{\circ})$	3.3 ± 3.2	3.9 ± 3.8	0.61 ± 0.12	R07-53
48	1 $^{\text{h}}34^{\text{m}}36^{\text{s}}.4$, 30°40'20"4	-192	0.22	7.5 ± 1.7	$105 \times 65(68^{\circ})$	5.6 ± 1.2	11.1 ± 2.5	0.18 ± 0.02	R07-136 ^a
49	1 $^{\text{h}}33^{\text{m}}38^{\text{s}}.9$, 30°32'49"7	-127	0.22	3.1 ± 4.3	$80 \times 63(129^{\circ})$	2.3 ± 3.2	1.5 ± 2.1	>0.49	G11-41
50	1 $^{\text{h}}33^{\text{m}}35^{\text{s}}.9$, 30°42'09"7	-194	0.22	7.2 ± 4.2	$111 \times 56(98^{\circ})$	5.0 ± 3.1	8.4 ± 5.3	0.42 ± 0.11	...
51 ^b	1 $^{\text{h}}33^{\text{m}}33^{\text{s}}.4$, 30°37'06"3	-142	0.22	5.3 ± 3.5	$97 \times 54(84^{\circ})$	3.1 ± 1.5	3.8 ± 1.8	0.38 ± 0.03	G11-89
52	1 $^{\text{h}}34^{\text{m}}07^{\text{s}}.1$, 30°39'23"7	-202	0.21	8.8 ± 6.6	$107 \times 62(17^{\circ})$	2.4 ± 1.3	14.6 ± 8.1	0.39 ± 0.06	R07-40, G11-173
53	1 $^{\text{h}}33^{\text{m}}23^{\text{s}}.5$, 30°31'58"4	-121	0.21	11.3 ± 1.8	$80 \times 69(110^{\circ})$	8.3 ± 1.9	22.2 ± 5.0	0.32 ± 0.03	R07-90, G11-40
54	1 $^{\text{h}}34^{\text{m}}12^{\text{s}}.7$, 30°48'30"3	-256	0.21	8.0 ± 2.8	$78 \times 62(174^{\circ})$	9.1 ± 2.8	9.5 ± 2.9	0.33 ± 0.05	R07-89, 93, G11-254, 258
55	1 $^{\text{h}}34^{\text{m}}04^{\text{s}}.7$, 30°48'59"8	-251	0.20	4.9 ± 2.2	$126 \times 47(152^{\circ})$	3.0 ± 2.2	...	0.32 ± 0.02	R07-87, G11-250
56	1 $^{\text{h}}33^{\text{m}}43^{\text{s}}.8$, 30°38'57"8	-150	0.20	6.0 ± 3.2	$82 \times 38(60^{\circ})$	2.1 ± 1.0	...	0.33 ± 0.03	G11-93
57	1 $^{\text{h}}33^{\text{m}}57^{\text{s}}.9$, 30°46'35"2	-246	0.20	4.6 ± 1.7	$57 \times 38(47^{\circ})$	1.3 ± 0.4	...	>0.37	G11-235, 243
58 ^b	1 $^{\text{h}}33^{\text{m}}51^{\text{s}}.4$, 30°35'53"8	-146	0.19	16.1 ± 6.3	$47 \times 40(84^{\circ})$	2.9 ± 1.4	...	0.48 ± 0.09	G11-141</

Table 2
(Continued)

GMC ID	R.A., Decl. (J2000.0)	V_{LSR} (km s $^{-1}$)	T_{mb} (K)	ΔV_{FWHM} (km s $^{-1}$)	$A_{\text{maj}} \times A_{\text{min}}$ (pc \times pc)	$L'_{\text{CO}(3-2)}$ (10^4 K km s $^{-1}$ pc 2)	M_{vir} ($10^5 M_{\odot}$)	$R_{3-2/1-0}$	Cross ID
(1)	(2)	(3)	(4)	(5)	(6)	(7)	(8)	(9)	(10)
66	1 ^h 34 ^m 10 ^s 8, 30°37'08"0	-166	0.16	6.5 ± 1.9	50 × 36(59°)	1.2 ± 0.4	...	0.18 ± 0.02	R07-69, G11-162
67	1 ^h 33 ^m 44 ^s 8, 30°32'06"9	-106	0.16	11.9 ± 6.4	65 × 44(156°)	3.5 ± 2.2	...	>0.69	R07-68, G11-21
68	1 ^h 34 ^m 10 ^s 2, 30°49'48"5	-260	0.15	8.6 ± 3.4	134 × 52(16°)	3.6 ± 1.4	10.1 ± 3.9	0.26 ± 0.04	R07-103, G11-262
69	1 ^h 34 ^m 02 ^s 5, 30°48'39"6	-255	0.15	5.3 ± 4.0	46 × 37(64°)	0.8 ± 0.6	...	0.29 ± 0.04	G11-257
70	1 ^h 33 ^m 59 ^s 6, 30°37'12"2	-171	0.14	7.9 ± 3.6	50 × 44(71°)	1.1 ± 0.4	...	0.43 ± 0.16	G11-167
71 ^b	1 ^h 33 ^m 22 ^s 6, 30°32'14"3	-141	0.13	16.6 ± 5.4	47 × 33(93°)	1.8 ± 1.2	G11-136

Notes. Column 1: GMC ID in order of decreasing peak intensity in spectrum. Column 2: intensity-weighted peak position R.A., decl. Column 3: observed local standard of rest (LSR) velocity of the peak intensity. Column 4: peak intensity in T_{mb} . Column 5: FWHM line width. Column 6: non-deconvolved major/minor axes and position angle in parentheses (measured counterclockwise from west to north). Column 7: CO($J = 3-2$) luminosity. Column 8: virial mass. Note that virial masses of 27 GMCs are not shown when the minor axis of the GMC is smaller than the beam size. Column 9: averaged $R_{3-2/1-0}$ over the extent of the GMC. Column 10: cross identifications with other catalogs. R07- n : from Rosolowsky et al. (2007). G11- n : from Gratier et al. (2012).

^a A single GMC in the Rosolowsky et al.’s (2007) catalog appears to be composed of more than two GMCs in our catalog.

^b GMCs at the edge of the field of view. The provided values are just lower limits.

smaller than the beam size, and thus the averaged R_{deconv} and M_{vir} should be regarded as upper limits. These averaged values are within the typical range as traced by CO($J = 1-0$) in LGGs (Fukui & Kawamura 2010).

Compared to the high-resolution CO($J = 3-2$) observations toward clumps in LMC, the R_{deconv} and M_{vir} of M33 GMCs are larger than the typical values of LMC clumps, i.e., $R_{\text{deconv}} = 1.1-12.4$ pc and $M_{\text{vir}} = 4.6 \times 10^3-2.2 \times 10^5 M_{\odot}$ (Minamidani et al. 2008). This is likely only due to our more limited spatial resolution, because the ΔV_{FWHM} of M33 GMCs is similar to that of the clumps at high resolution, ΔV_{FWHM} of ~ 7 km s $^{-1}$. This suggests that the M33 GMCs obtained in this work are composed of a single or a few small clumps at a similar velocity, but not a large amount of clumps.

3.1.1. CO($J = 3-2$) and CO($J = 1-0$) Distribution and $R_{3-2/1-0}$

The CO($J = 3-2$) and CO($J = 1-0$) integrated intensity maps and also the CO intensity ratio ($R_{3-2/1-0}$) map for each individual GMC, with a common 25'' resolution, are shown in panels (a)-(c) of Figures 13–16 and Figure 18. The integrated intensity maps of CO($J = 3-2$) emission have been created by using the channel maps where the emission is above $2\sigma_{\text{ch}}$. The integrated intensity maps of CO($J = 1-0$) emission have been binned over the same velocity ranges as that of CO($J = 3-2$) emission.

We find a general trend that the distribution of CO($J = 3-2$) emission and peaks are similar to that of CO($J = 1-0$) (e.g., GMC-3 and GMC-5 in Figure 18, available in the online journal). However, in some cases ($\sim 28\%$), the CO($J = 3-2$) emission for some GMCs shows more compact distribution (e.g., GMC-1 in Figure 15, GMC-8 in Figure 14). In other GMCs ($\sim 11\%$), the CO($J = 3-2$) emission peak is offset from the CO($J = 1-0$) emission peak by over half HPBW (e.g., GMC-1 in Figure 15, GMC-7 in Figure 18). A further description of the spatial comparison between CO emission and massive SF sites is presented later in Section 3.5.

We have calculated $R_{3-2/1-0}$ by dividing the CO($J = 1-0$) map by the CO($J = 3-2$) map, after masking the region where the CO($J = 1-0$) emission is below 3σ in its integrated intensity map. Note that each $R_{3-2/1-0}$ map is masked except inside the boundary of the GMC, to avoid confusion with neighboring GMCs.

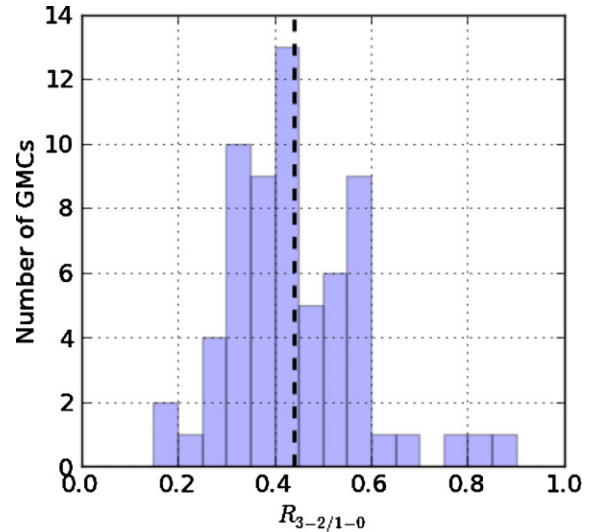


Figure 3. Distribution of average $R_{3-2/1-0}$ over each GMC. The GMCs at the edge of the observed fields or with underivable $R_{3-2/1-0}$ were discarded. The dashed line represents the average value, 0.43.

(A color version of this figure is available in the online journal.)

The $R_{3-2/1-0}$ values across GMCs vary greatly. Some GMCs are found to have a gradient of $R_{3-2/1-0}$, while others have a relatively constant ratio. The averaged $R_{3-2/1-0}$ is measured inside the boundary of GMCs and is provided in Column (9) of Table 2. The CO($J = 3-2$) emission for four GMCs (GMC-49, 56, 57, and 70) have been detected with significant signal-to-noise ratio but the CO($J = 1-0$) emission has not been detected at the same position. In case that the $R_{3-2/1-0}$ for these GMCs is uncertain, we calculate the lower limit of $R_{3-2/1-0}$ at the CO($J = 3-2$) emission peak (see captions in each figure). Figure 3 shows the histogram of $R_{3-2/1-0}$ for the 65 GMCs. The averaged $R_{3-2/1-0}$ ranges from 0.18 to 0.89, with a mean of 0.43. High ratios, $R_{3-2/1-0} > 0.6$, are found at four GMCs: GMC-1, GMC-7, GMC-34, and GMC-42, which are located around the GHRs (NGC 604, NGC 595) and the vicinity of the galaxy center.

3.2. Identification of YSGs and Their Ages

The color-magnitude diagram (CMD) is a powerful tool for providing insight into the age of the stellar component in a region

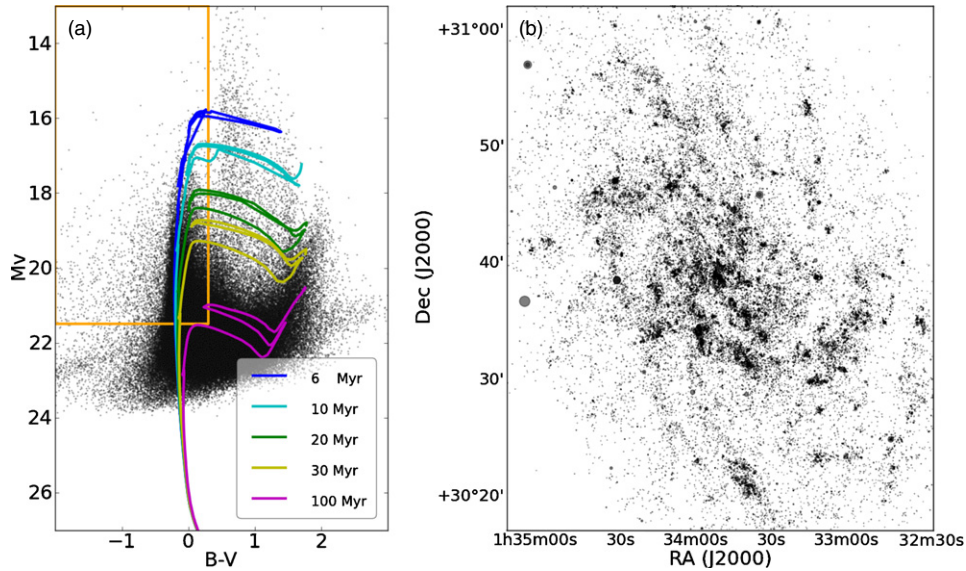


Figure 4. (a) The color–magnitude diagram of the entire disk of M33. The five lines represent isochrone tracks of 6 Myr (blue), 10 Myr (cyan), 20 Myr (green), 30 Myr (yellow), and 100 Myr (pink). A metallicity of $0.5 Z_{\odot}$ was used. The orange boundary (horizontal and vertical lines) indicates our color and magnitude selection criteria, $(B - V)_0 < 0.3$ and $M_V < 21.5$. (b) The spatial distribution of identified young stars, selected using the same color and magnitude criteria. Note that the point sizes in this plot are proportional to the stellar brightness in V band.

of interest. Next we describe the method to identify YSGs as well as how to estimate their ages using the CMD. The results are then used to investigate the spatial correlation between the YSGs and the GMCs identified in Section 3.1.

3.2.1. Extraction of Young Stars

We have created the V magnitude– $(B - V)$ CMD (i.e., $M_V - (B - V)_0$ diagram) for the disk of M33 using the photometry catalog described in Section 2.3. To obtain intrinsic absolute magnitudes and then accurate ages, the photometric measurements must be corrected for two sources of reddening: the foreground extinction from our Galaxy and the internal reddening due to the interstellar matter in the disk of M33. We adopt the foreground galactic extinctions in the B and V bands of 0.181 and 0.139 mag, respectively (Schlegel et al. 1998).

The reddening $E(B - V)$ has been measured toward some individual clusters in M33, and ranges from 0.06 to 0.3 mag, with a typical value of 0.10 (Chandar et al. 1999; Park & Lee 2007). Due to the different density structures of the GMCs, it is necessary to consider a variable internal reddening correction. This is especially important if the stars are embedded or lie behind the GMC, as the visual extinction is then expected to be higher (e.g., Pineda et al. 2010). The exact correction for a given line of sight is rather uncertain, but we have used the available $E(B - V)$ values obtained for some clusters, and the typical value of $E(B - V) = 0.10$ (Chandar et al. 1999; Park & Lee 2007) for the remaining stellar groups. The ratio of total to selective extinction $R_V = A_V/E(B - V) \simeq 3.1$ in our Galaxy (Savage & Mathis 1979) is used to obtain the visual extinction A_V .

We have used the theoretical isochrones in the Padova stellar population synthesis models (Marigo et al. 2008; Girardi et al. 2010, and references therein) to estimate the age of the stars. The adopted distance to M33 (840 kpc; Freedman et al. 2001) corresponds to a distance modulus $(m - M)_0 = 24.6$. Note that the metallicity (Z) varies from $0.6 Z_{\odot}$ in the central region to $0.4 Z_{\odot}$ at 5 kpc galaxy radius (Bresolin 2011).

Figure 4(a) shows a $M_V - (B - V)_0$ diagram for the stars in M33 with five stellar isochrones from the Padova models (Marigo et al. 2008; Girardi et al. 2010, and references therein),

assuming $Z = 0.5 Z_{\odot}$, ages of 6, 10, 20, 30, and 100 Myr, and an average internal extinction correction of $A_V \sim 0.22$ (Massey et al. 2007; Bastian et al. 2007). Massey et al. (2006, 2007) have estimated that $\sim 40\%$ of stars have $(B - V)_0$ between 0.3 and 1.0, but M_V in the range of 14.6–19.6 are likely foreground objects (Bastian et al. 2007). Taking into account photometric errors and foreground galactic extinction, the criterion of $(B - V)_0 < 0.3$ is chosen to avoid the foreground stars. The faint limit of the V -band magnitude of $M_V < 21.5$ is set to select only young massive stars (<100 Myr). The minimum (initial) stellar masses at $M_V \sim 21.5$ for ages of 6, 10, 20, 30, 100 Myr correspond to 14, 13, 10, 8, and $5 M_{\odot}$, respectively. The orange boundary in Figure 4(a) indicates our selection criteria, $(B - V)_0 < 0.3$ and $M_V < 21.5$, an area that should represent young stars.

The selected young stars are plotted in Figure 4(b), where the point size in the plot is proportional to the stellar brightness in V band. These young stars (<100 Myr) are found to be distributed in a structure with two main arms and several weak multiple arms, which is in good agreement with Ivanov & Kunchev (1985).

3.2.2. Young Stellar Number Density Map, Identification of YSGs and Their Ages

We describe the method to search for YSGs and how to estimate their ages. The term “YSGs” refers to the concentration of young stars selected using the criteria in Section 3.2.1. These will include both (young) star clusters as well as OB associations. Generally, a star cluster is defined to be a gravitationally bound system of several stars or more, whose concentration is larger than that of the surrounding stellar background, with a typical size of a few parsecs to tens of parsecs (e.g., Hwang & Lee 2008, and references therein). The definition of an OB association is usually a single, loosely bound, or unbound concentration of early-type luminous stars, typically extending several tens to over a hundred parsecs (e.g., Gouliermis et al. 2000, and references therein). The typical masses of young (<10 Myr) clusters and associations are $10\text{--}10^4 M_{\odot}$ and $10^3\text{--}10^6 M_{\odot}$, respectively (e.g., Hunter et al. 2003; Kaleida & Scowen 2010). Here, we do not aim to distinguish between them because our interest is

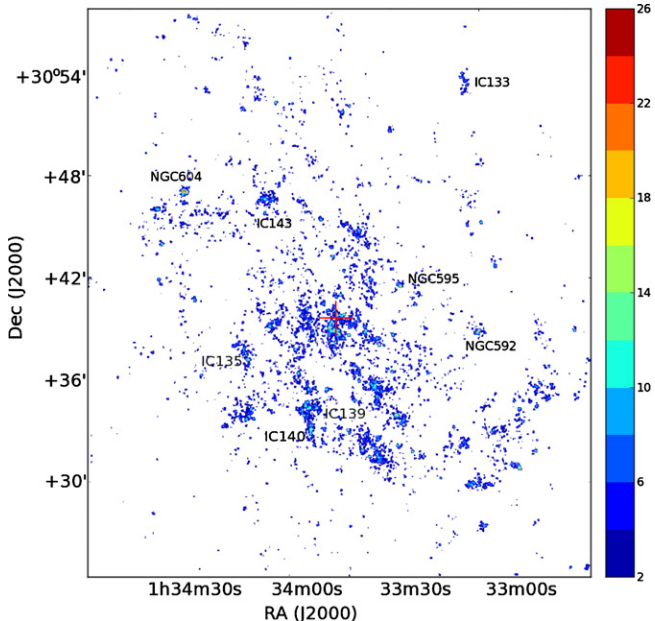


Figure 5. Number density (n^*) map of young stars shown in Figure 4(b), measured in $30\text{ pc} \times 30\text{ pc}$ area. The color range spans from 2 to 26 stars per area, in two stars per area color steps. This corresponds to $0.002\text{--}0.031$ stars per pc^2 , in 0.002 stars per pc^2 steps. The number density of $n^* < 2$ stars per area is not shown. Prominent H II regions are also labeled for reference. A cross symbol in the middle of the image represents the galaxy center.

to investigate the collective properties of YSGs associated with GMCs.

In previous studies, clusters or associations have been selected to be stellar groups just by visual inspection, and therefore the selection may have been subjective. Recently, a more objective approach has been carried out by Gouliermis et al. (2000, 2010), who have performed a stellar cluster identification in NGC 6822 and the LMC using the stellar surface density map, and have shown the hierarchical structure of blue stellar clusters.

To select YSGs in an objective manner for M33 as well, we define them as an excess in the number of young stars per unit of area (n^*) following Gouliermis et al.’s (2000, 2010) approach. We set the unit of area to the same scale as the pixel size of CO($J = 3\text{--}2$) map, a $8'' \times 8''$ box (corresponding to $\sim 30\text{ pc} \times 30\text{ pc}$), which is comparable to the typical GMC size. The pixel size of the stellar number density map is set to half of the pixel size of the CO($J = 3\text{--}2$) map, 15 pc. Figure 5 shows the number density map of young stars per each $30\text{ pc} \times 30\text{ pc}$ area in M33 disk. It becomes more clear than in Figure 4(b) that most of the regions with $n^* > 2$ stars per unit area are distributed along the spiral arms of M33. The maximum value of stellar number density in M33 is found in the center of NGC 604, $n^* = 28$ stars per area. Overdensity regions ($n^* > 15$ stars per area) coincide with prominent H II regions such as NGC 604, NGC 595, NGC 592, IC 135, IC 139, IC 140, and the galaxy center, as labeled in Figure 5.

Next we compare the number density map with other wavelength data. Figure 6 shows the M33 disk in CO($J = 1\text{--}0$), $24\text{ }\mu\text{m}$, H α , and far-UV (FUV). The background-subtracted FUV map is a reproduction from Verley et al. (2010). Interestingly, the distributions of the molecular gas traced by CO($J = 1\text{--}0$) in Figure 6(a) and the young stars in Figure 5 exhibit slightly different patterns between the northern and the southern sides of the disk: molecular gas is more abundant in the northern side of the disk, while the opposite is true for young

stars. Note that this asymmetrical pattern of the young stellar distributions is not because the photometric depth is inhomogeneous over the disk, as the completeness limits are similar (below $V \sim 21.5$ mag) both in the northern and southern disks.

The distributions of $24\text{ }\mu\text{m}$ and H α emissions show multiple spiral arms similarly to the density map of young stars, but their spatial distribution patterns are not always similar: the $24\text{ }\mu\text{m}$ and H α emissions are enhanced at GHRs such as NGC 604 and NGC 595 compared to other disk regions, while the surface density map of young stars is more pronounced along the spiral arms (Figures 6(b) and (c)). The distribution of the young star number density is remarkably similar to that of the FUV emission in Figure 6(d), which traces the spiral structure and reproduces the north–south asymmetry. This is consistent with FUV being a diagnostic of the younger (30–100 Myr) stellar population (Verley et al. 2009, 2010).

In this work, we adopt five young stars per $30\text{ pc} \times 30\text{ pc}$ area as the minimum surface stellar number required to be classified as a YSG, and then we estimate its age from the CMD, assuming that stars are coeval. First, we search a region with a peak of $n^* > 5$ stars per area around each GMC, then determine the extent of the YSG at a level of $n^* = 2$ stars per unit area. A Gaussian is then fitted to the radial profile of the young stellar distribution down to $n^* > 2$, and the extent of YSGs is set as the FWHM of that Gaussian fit assuming a circular shape (r_{cl}). Second, we have created the $M_V - (B - V)_0$ diagrams for the stars contained within the radius of r_{cl} . Finally, we estimate their age using the Padova models.

As an example, Figure 7(a) shows the number density map of young stars, overlaid on the CO($J = 3\text{--}2$) map of the NGC 604 region. Three GMCs are identified, GMC-34, GMC-1, and GMC-27, from north to south in this region. We find three peaks of $n^* > 5$ stars per area around these GMCs, at position $(\alpha_{J2000}, \delta_{J2000}) = (1^{\text{h}}34^{\text{m}}31^{\text{s}}.4, 30^{\circ}47'48''.0)$, $(1^{\text{h}}34^{\text{m}}33^{\text{s}}.4, 30^{\circ}47'03''.5)$, and $(1^{\text{h}}34^{\text{m}}33^{\text{s}}.0, 30^{\circ}46'23''.8)$ from north to south, which we refer to as YSG-71, YSG-73, and YSG-72, respectively. The radii of these YSGs are measured to be $r_{\text{cl}} = 9''.5$ (39 pc), $21''.2$ (86 pc), and $10''.4$ (42 pc), respectively.

Next, we derive ages for each YSG by fitting theoretical isochrones to the CMDs of resolved stars. Figure 8 shows the CMD of the three identified YSGs above, YSG-71, YSG-72, and YSG-73. Dot symbols represent the stars within the radius of r_{cl} and the lines represent the Padova theoretical isochrone tracks, assuming a metallicity of $0.5 Z_{\odot}$. Solid lines represent the upper limit of the estimated ages, regarding the magnitude and color of the brightest main-sequence (MS) star as MS turnoffs for a young star group. In this case, the more massive stars are assumed to have already evolved from the MS lines at $(B - V)_0 \sim 0$ and less massive stars are still in the MS. Dashed lines represent the lower limit of the estimated ages, considering that all stars in the YSGs are still in the MS at $(B - V)_0 \sim 0$, without any more massive stars in the group evolving to red giant branches. Although chances are low that these massive stars are detected at redder colors, because the more massive the stars the faster they evolve, no detection of stars at $(B - V)_0 > 0$ can suggest that more massive stars have not existed before. Note that in either case, we have used only stars at $(B - V)_0 < 0.3$ to avoid foreground stars (Section 3.2.1). The measurable age limit of these YSGs using the Padova models is 3 Myr. In this way, the estimated ages of the three YSGs YSG-71, YSG-72, and YSG-73 are in the range of 3–28 Myr, 3–28 Myr, and 3–5 Myr, respectively. The first two YSGs include a smaller number of stars (11 and 21 O stars for YSG-71 and YSG-72, respectively)

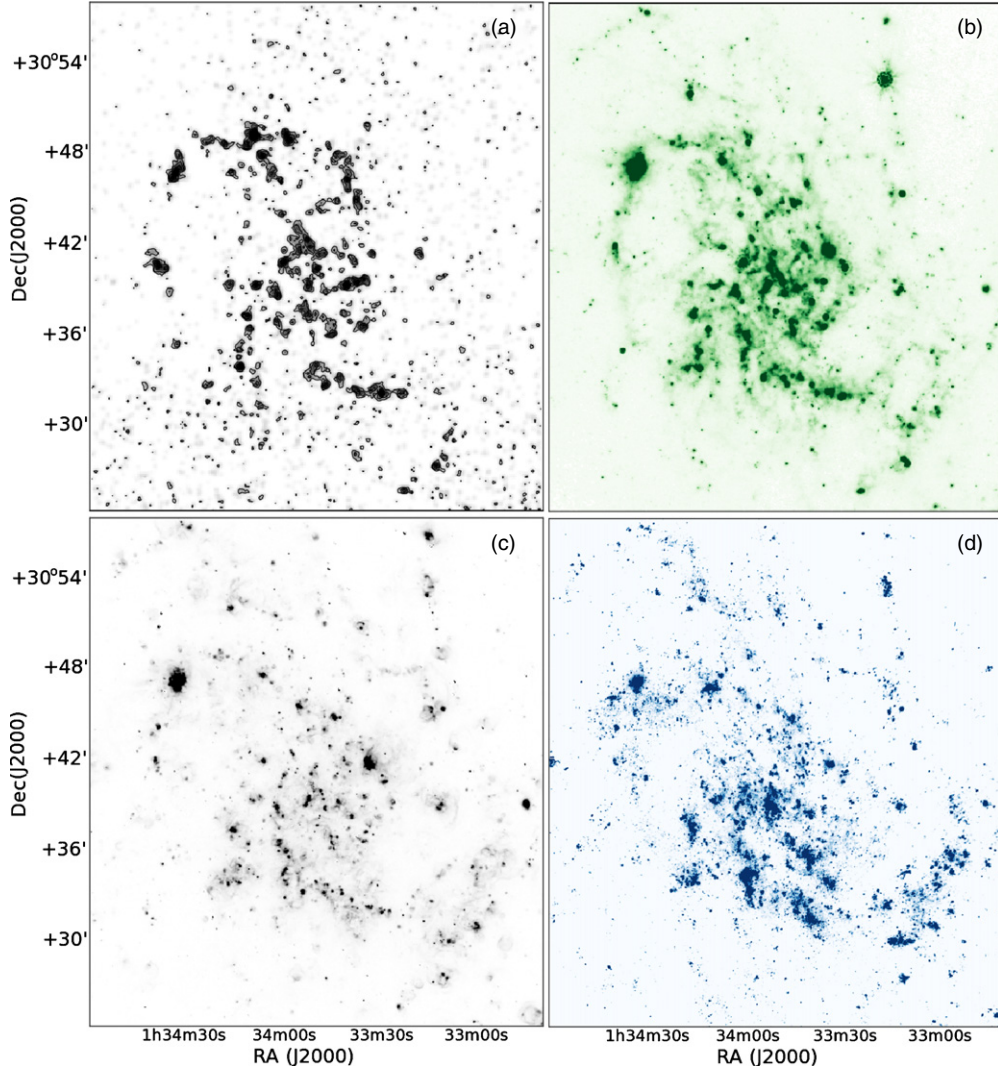


Figure 6. (a) CO(1–0) integrated intensity map (see Section 2.2). Contour levels are 1σ , 2σ , 3σ , ..., 8σ , where the noise level $1\sigma = 1.7 \text{ K km s}^{-1}$. Images of (b) $24 \mu\text{m}$, (c) H α , and (d) FUV (See Sections 2.3 and 3.2.2.)

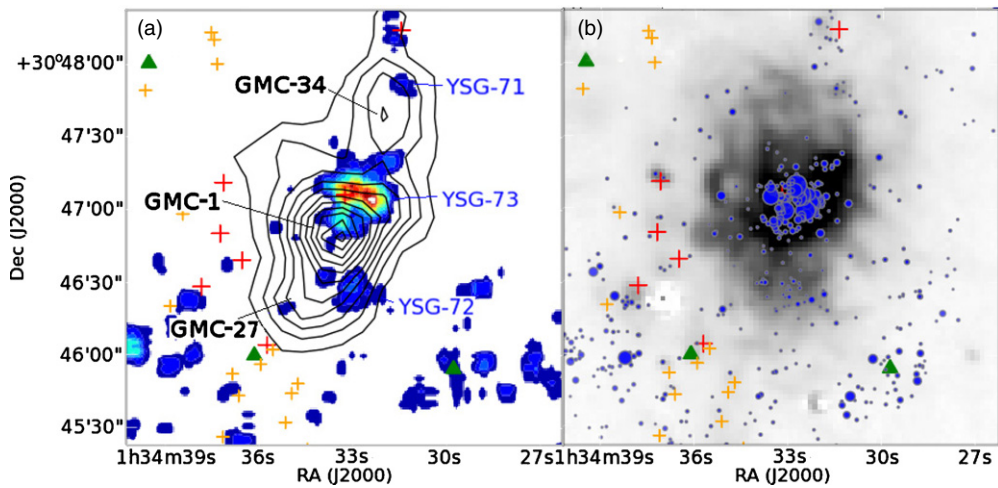


Figure 7. (a) The stellar density map toward NGC 604, overlaid with CO($J = 3 - 2$) contours. Contour levels are 1, 2, 3, ..., and 13 K km s^{-1} . YSG-XX and GMC-XX are the IDs from our young stellar group and CO($J = 3 - 2$) GMC catalogs. The crosses are the H II regions from Courtes et al. (1987; red), and Hodge et al. (1999) and Wyder et al. (1997) (orange). The green triangles are the $24 \mu\text{m}$ sources in Verley et al. (2007). The color range is the same as in Figure 5. (b) The distribution of individual young stars overlaid on the grayscale image of H α emission of the NGC 604 region. The blue circles represent young stars which are selected with our color and magnitude criteria (see Figure 4) and their sizes are proportional to the stellar brightness in V band. Note that only the stars inside the radius of $90''$ from the center of the NGC 604 are shown.

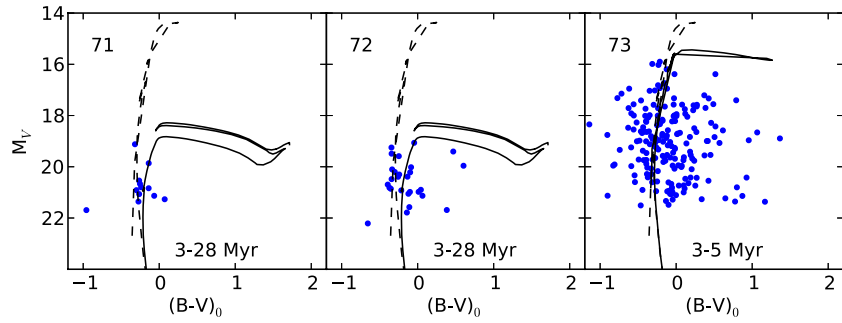


Figure 8. Color–magnitude diagrams of the three identified YSGs around NGC 604: YSG-71, YSG-72, and YSG-73 (NGC 604), from the left to the right panel. The dots denote the stars within the selection radius, 9'.5 (39 pc), 10'.4 (42 pc), and 21''.2 (86 pc), respectively, which correspond to the extent at a $n^* = 2$ stars per area level. The solid and dashed lines are the Padova theoretical isochrone tracks of the upper and lower limits of the estimated age, respectively. The identification number in the catalog and the derived age of each YSG are shown at the upper left and lower right corners of each panel, respectively.

(A color version of this figure is available in the online journal.)

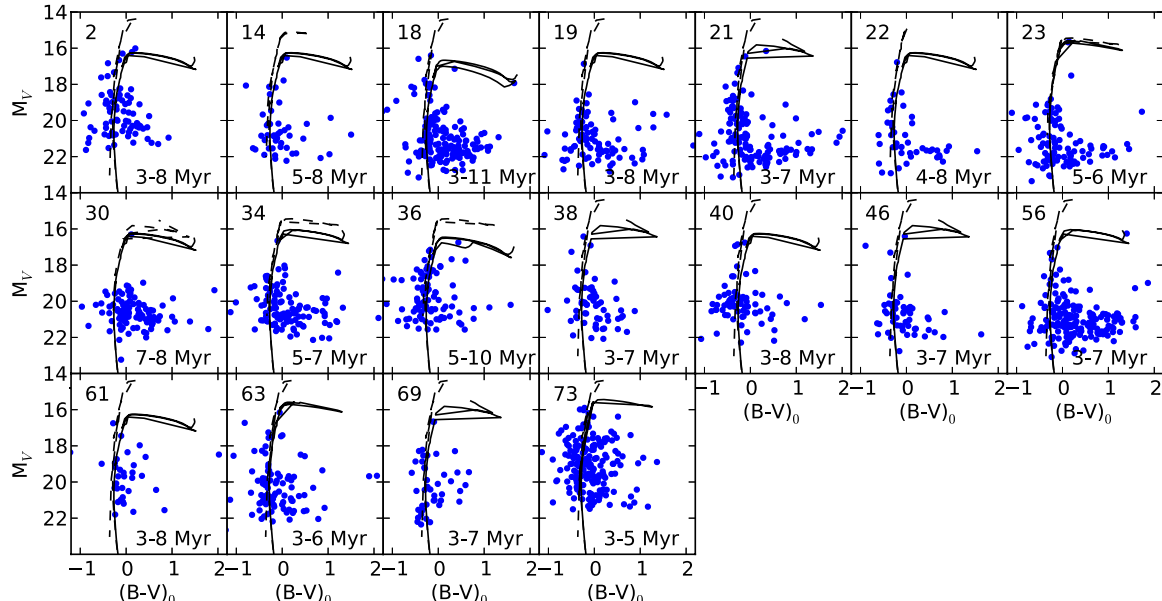


Figure 9. Color–magnitude diagrams of 18 YSGs (among the 75 in the catalog), whose upper limit ages are estimated to be less than 10 Myr. Dots denote the stars within the selection extent (r_{cl}) in Table 3. The lines and labels are the same as in Figure 8.

(A color version of this figure is available in the online journal.)

and mostly less bright stars ($M_V \gtrsim 19$ mag), which makes a larger uncertainty in the estimations.

Figure 7(b) shows the distribution of the young stars, overlaid on the H α map (gray scale). The size of the blue circle representing each star is proportional to the brightness in the V band, that is, the larger the brighter. Many bright young stars are found in YSG-73 and concentrated in the center of the H II region. In fact, NGC 604 is known to be the most luminous and massive H II region in M33, containing more than 200 O-type stars (Drissen et al. 1993; Hunter et al. 1996; González Delgado & Pérez 2000; Bruhweiler et al. 2003). The other two YSGs (YSG-71 and YSG-72) do not have cross identifications in previous cluster catalogs, but are included in previous star complex and OB association catalogs (No. 46 in Ivanov 2005; Humphreys & Sandage 1980).

3.2.3. The Catalog of YSGs

We have identified 75 YSGs in M33 and have estimated their ages as described in Section 3.2.2. Note that only YSGs associated with the identified GMCs are included (see Section 3.3).

Figures 9–11 show the CMDs of 75 YSGs with the adopted Padova theoretical isochrone tracks. Similarly to Figure 8, solid and dashed lines represent the upper and lower limits of the estimated ages. Blue dots represent the stars within the r_{cl} of the YSGs. In Figures 9–11, we show the CMDs of 18 YSGs younger than at most 10 Myr, 17 YSGs older than at least 10 Myr, and the remaining 40 YSGs, respectively.

Table 3 shows the properties of the YSGs identified in our catalog, including positions, size (r_{cl}), number of O stars, V magnitude of the brightest O star in the YSG, applied reddening correction, estimated age, and cross identifications. The number of O stars are counted only for those within our criterion on the M_V –($B - V$)₀ diagrams, i.e., $(B - V)_0 < 0.3$ and $M_V < 21.5$. Note that this stellar age provides just an upper limit for the YSGs, partly because reddening correction is uncertain. Twenty-three YSGs do not coincide with previously identified clusters, but are included in star complex and OB association catalogs (Ivanov 2005; Humphreys & Sandage 1980). The remaining are found to have cross identifications with previous cluster catalogs (SM; Park & Lee 2007; San Roman et al. 2010).

The radii of the YSGs range from 6''.6 to 22''.4 (27–91 pc) and the average is 11'' (46 pc). The number of O stars in a

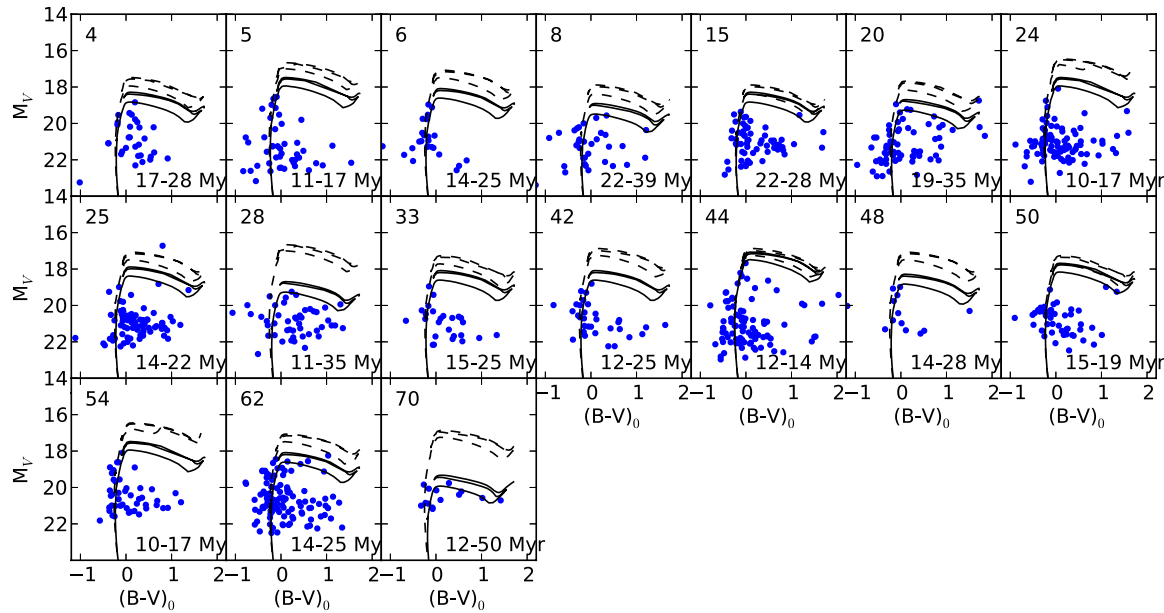


Figure 10. Same as Figure 9 but for 17 YSGs (among 75 in the catalog), whose ages are estimated to be older than 10 Myr.

(A color version of this figure is available in the online journal.)

YSG ranges from 9 to 169 stars. The total stellar mass of the YSGs are estimated to be $10^{3.5}–10^{4.7} M_{\odot}$, assuming that the YSGs are characterized by a Salpeter initial mass function (IMF) (slope -2.35), with masses spanning $0.1–58 M_{\odot}$. These sizes and masses are comparable to the typical values of OB associations (e.g., Bica & Schmitt 1995; Battinelli et al. 1996; Kaleida & Scowen 2010). It is possible to estimate the stellar spectral type of the primary ionizing star contained in a YSG from the brightest V -magnitude and $(B - V)_0$ color. The most massive stars are found in YSG-21 and YSG-73 and their masses are estimated to be $51 M_{\odot}$, corresponding to O3.5V (Martins et al. 2005). The brightest stars in YSG-39 and YSG-60 are less massive than in any other YSGs, $8 M_{\odot}$ (corresponding to B2V). The latter is comparable to small clusters in our Galaxy and the LMC that can be ionized by a single mid-O or B0 star (e.g., Panagia & Ranieri 1973; Wilcots 1994). The ages of the YSGs are estimated to be in the range between 4 ± 1 Myr and 31 ± 19 Myr, with an average of 12 ± 5 Myr.

We can compare the ages with other catalogs. Although the YSGs in our catalog do not fully overlap with the clusters whose ages have been previously determined (SM; PPL; SSGH), only five YSGs coincide, YSG-1, YSG-13, YSG-41, YSG-63, and YSG-67. The previously derived ages are 25^{+38}_{-14} Myr (PPL), 13 Myr (SM), 16^{+4}_{-3} Myr (PPL) or 21 Myr (SM), 5 Myr (SM) or 13^{+7}_{-5} Myr (PPL), and 40^{+60}_{-24} Myr (PPL), respectively, while they are 9 ± 2 Myr, 11 ± 5 Myr, 9 ± 2 Myr, 5 ± 2 Myr, and 14 ± 11 Myr in our estimation. Compared to the results for YSG-1, YSG-41, YSG-63, and YSG-67 in PPL who have used a similar method, we note that our estimations of ages are slightly younger than them but are consistent within the uncertainties. This slight difference is mostly because they have used a small member star selection radius (within $1''–2''$) of a compact stellar cluster and also because they have applied different theoretical isochrones in the Padova models, corresponding to $Z = 0.2 Z_{\odot}$. Besides, even though a cluster in their catalogs is associated with one of our YSGs, in general it only represents a small portion of the YSG, and thus it is not clear in principle whether they represent exactly the same entity. For the ages of the

other two YSGs (clusters) in known GHRs (NGC 595 and NGC 604), YSG-2 and YSG-73, they had been previously estimated to be $4–6$ Myr (Drissen et al. 1990; Malumuth et al. 1996) and $3–5$ Myr, respectively, using optical spectroscopy combined with an instantaneous starburst model (e.g., González Delgado & Pérez 2000). The ages of these young clusters are in good agreement with our results, 6 ± 3 Myr and 4 ± 1 Myr, respectively.

3.3. H II Regions and YSGs Associated with GMCs

In this section, we investigate the associations of $\text{H}\alpha$, $24 \mu\text{m}$ sources, and the identified YSGs, with the GMCs. These associations are listed in Table 4. $\text{H}\alpha$ regions are tracers of the younger stellar population (< 10 Myr), while $24 \mu\text{m}$ sources represent massive SF sites embedded in dust. When the extent of $\text{H}\alpha$ regions, $24 \mu\text{m}$ sources, and YSGs are confined within the boundary of a GMC, they are treated as being associated with the GMC.

The $\text{H}\alpha$ region catalogs (Boulesteix et al. 1974; Courtes et al. 1987; Hodge et al. 1999) include those $\text{H}\alpha$ regions with $\text{H}\alpha$ luminosities larger than $10^{34.4} \text{ erg s}^{-1}$ (Wyder et al. 1997). Therefore, the sensitivity of the survey is high enough to detect the equivalent to a single O9V-type star (Martins et al. 2005), assuming a standard relation between ionizing photon rates and $\text{H}\alpha$ luminosities (Mayya & Prabhu 1996, and references therein). For the $24 \mu\text{m}$ sources, the faint end of the $24 \mu\text{m}$ luminosity in the catalog (Verley et al. 2007) is $\sim 10^{37.7} \text{ erg s}^{-1}$, corresponding just to an $\text{H}\alpha$ region illuminated by a single B1.5V star. Note that the $24 \mu\text{m}$ source catalog includes discrete sources such as $\text{H}\alpha$ regions, supernovae remnants, and planetary nebulae, but most of the $24 \mu\text{m}$ sources are classified as $\text{H}\alpha$ regions (Verley et al. 2007), which contain embedded young stellar clusters with ages of $3–10$ Myr (Sharma et al. 2011).

The $24 \mu\text{m}$ sources have generally corresponding $\text{H}\alpha$ emitting sources, but there are some cases of $24 \mu\text{m}$ sources without a corresponding $\text{H}\alpha$ source (see the last column in Table 4). All GMCs except GMC-60 are found to be associated with $\text{H}\alpha$

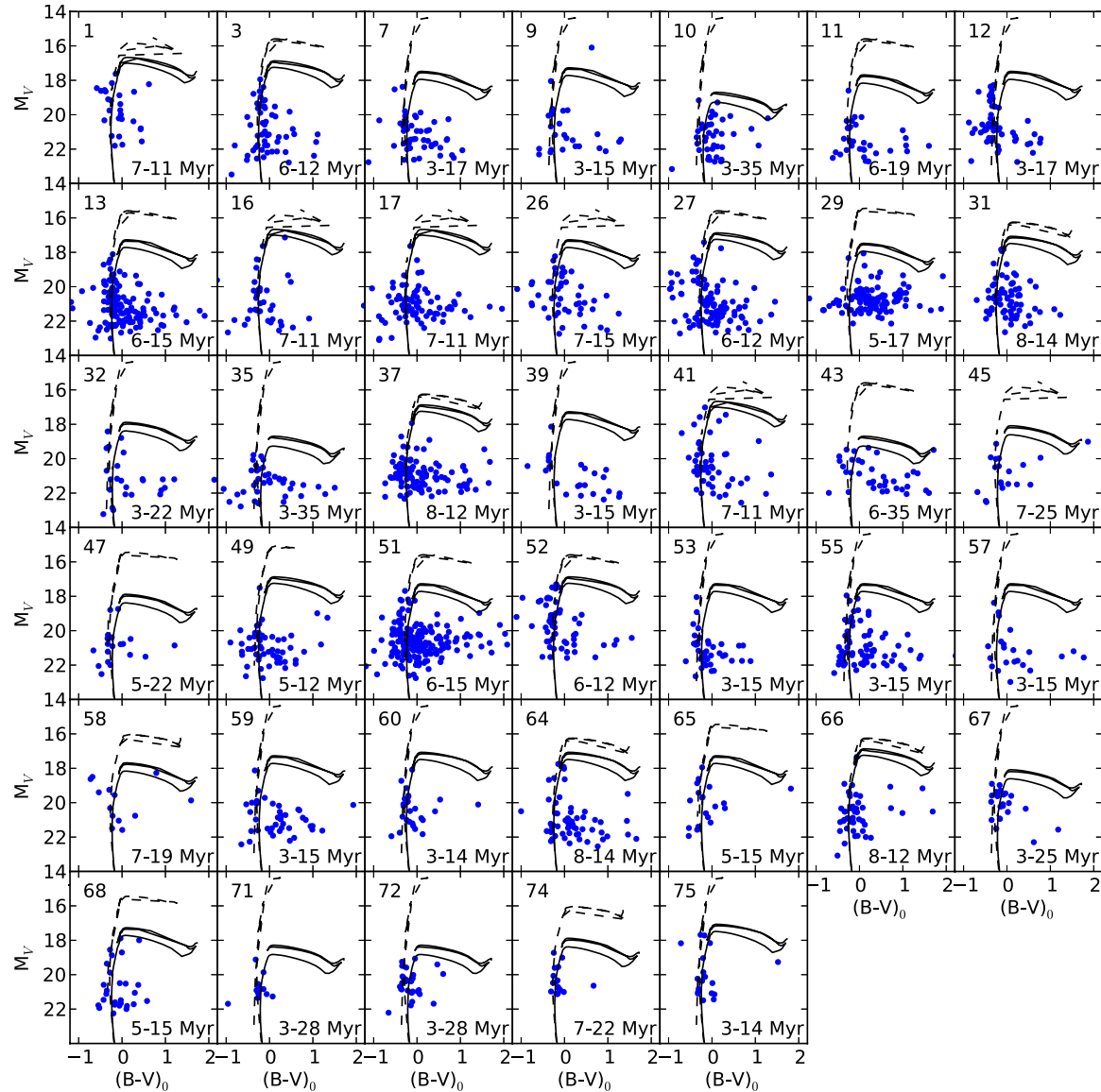


Figure 11. Same as Figure 9 but for the remaining 40 YSGs not included in Figures 9 and 10. A total of 25 of these are estimated to be younger than 15 Myr.
(A color version of this figure is available in the online journal.)

regions and/or 24 μm sources, while 51 GMCs are found to be associated with YSGs. In 10 GMCs no H II region exists but 24 μm sources have been identified, while in 16 GMCs there are H II regions without corresponding 24 μm sources.

The H α and 24 μm luminosities, $L(\text{H}\alpha)$ and $L(24 \mu\text{m})$, and SFRs for each GMC are also listed in Table 4, where the SFR for each GMC is calculated from the $L(\text{H}\alpha)$ and $L(24 \mu\text{m})$ using the relation between the extinction-corrected H α emission and the SFR (Calzetti et al. 2007). The $L(\text{H}\alpha)$ and $L(24 \mu\text{m})$ for each GMC are measured with a circular aperture of size equal to that of the associated GMC (100–400 pc diameter). These aperture photometry measurements include local background subtraction. Determination of the local background is done by fitting the emission over the aperture with Gaussian functions. These aperture sizes are similar to or larger than a typical H II region (1 pc–100 pc) and thus they may potentially contain several H II regions. A more careful local background subtraction for these H II regions would just result in even larger differences in luminosities between a small H II region and a large one because the

local background contamination tends to be systematically large at the faint end (Liu et al. 2011). The $L(\text{H}\alpha)$ and $L(24 \mu\text{m})$ range from 2.49×10^{35} to $7.67 \times 10^{39} \text{ erg s}^{-1}$, and from 1.67×10^{37} to $4.04 \times 10^{40} \text{ erg s}^{-1}$, respectively. The most luminous source both in H α and 24 μm emission is found at GMC-1, corresponding to NGC 604. The SFR of the M33 GMCs is characterized by a large scatter, ranging from 8.89×10^{-5} to $0.216 M_{\odot} \text{ yr}^{-1}$.

We estimate the averaged H α attenuation over a GMC (i.e., a few 100 pc scale) using $L(24 \mu\text{m})/L(\text{H}\alpha)$ ratio as a proxy (Prescott et al. 2007; Kennicutt et al. 2007). The H α attenuation is given by $A_{\text{H}\alpha} = 2.5 \log[1+0.038 L(24 \mu\text{m})/L(\text{H}\alpha)]$ (Calzetti et al. 2005; Prescott et al. 2007). We list $A_{\text{H}\alpha}$ in Table 4. The $A_{\text{H}\alpha}$ is generally low (less than 1 mag) and in good agreement with previous studies (Grossi et al. 2010; Sharma et al. 2011). The averaged $A_{\text{H}\alpha}$ is 0.4 mag ($A_V \sim 0.5$) and is consistent with the adopted extinction for individual YSGs in Section 3.2.1. Relatively highly obscured sources ($A_{\text{H}\alpha} > 2$ mag) are found in three GMCs: GMC-6, 15, and 68. The ages for the YSGs associated with these GMCs may be underestimated. Note that

Table 3
M33 Young Stellar Group Catalog

YSG ID	R.A., Decl. (J2000.0)	r_{cl} (")	N_{Ostar}	M_v (mag)	$E(B - V)$	Age (Myr)	Cross ID
(1)	(2)	(3)	(4)	(5)	(6)	(7)	(8)
1	01 ^h 33 ^m 30 ^s .2, 30°31'44".9	8.3	21	17.62	0.10 ^a	7–11	SM464, PL12, SSA1272
2	01 ^h 33 ^m 33 ^s .6, 30°41'27".6	12.5	67	16.01	0.20 ^a	3–8	NGC 595, PL57
3	01 ^h 33 ^m 34 ^s .3, 30°32'05".8	12.6	30	17.94	0.10	6–12	SSA1261, SSA1267, SSA1272
4	01 ^h 33 ^m 35 ^s .0, 30°37'02".4	7.4	17	18.84	0.10	17–28	SSA1284, SM113
5	01 ^h 33 ^m 35 ^s .2, 30°39'18".1	12.5	18	18.54	0.10	11–17	...
6	01 ^h 33 ^m 35 ^s .7, 30°42'32".2	8.9	18	18.96	0.10	14–25	SSA1285
7	01 ^h 33 ^m 35 ^s .9, 30°36'29".0	9.8	24	18.38	0.10	3–17	SM128
8	01 ^h 33 ^m 36 ^s .4, 30°31'49".1	8.0	15	19.70	0.10	22–39	SSA1294
9	01 ^h 33 ^m 36 ^s .8, 30°36'35".2	8.0	14	18.05	0.10	3–15	...
10	01 ^h 33 ^m 38 ^s .0, 30°32'01".7	<10.0	18	19.16	0.10	3–35	...
11	01 ^h 33 ^m 38 ^s .7, 30°32'07".9	8.0	11	18.60	0.10	6–19	...
12	01 ^h 33 ^m 39 ^s .3, 30°38'04".0	9.5	42	18.28	0.10	3–17	SSA1341, SSA1350
13	01 ^h 33 ^m 39 ^s .6, 30°32'37".2	17.2	67	18.11	0.10 ^a	6–15	SSA1343, SSA1345, PL139
14	01 ^h 33 ^m 40 ^s .5, 30°38'28".0	8.7	28	16.52	0.10	5–8	SSA1344 (SM545), SSA1361 (SM154)
15	01 ^h 33 ^m 42 ^s .2, 30°40'21".5	12.1	29	19.36	0.10	22–28	SSA1394, SSA1407
16	01 ^h 33 ^m 42 ^s .3, 30°33'00".2	9.3	22	17.64	0.10	7–11	SSA1406
17	01 ^h 33 ^m 43 ^s .1, 30°32'47".6	11.9	42	17.64	0.10	7–11	SSA1415
18	01 ^h 33 ^m 43 ^s .5, 30°39'05".7	17.0	65	16.40	0.10	3–7	SSA1430, SSA1416
19	01 ^h 33 ^m 44 ^s .3, 30°31'48".0	13.8	44	16.87	0.10	3–8	...
20	01 ^h 33 ^m 44 ^s .8, 30°33'08".2	11.4	23	18.94	0.10	19–35	...
21	01 ^h 33 ^m 44 ^s .9, 30°36'31".1	16.4	63	16.46	0.10	3–7	SM565
22	01 ^h 33 ^m 44 ^s .9, 30°35'53".5	9.9	25	16.78	0.10	4–8	...
23	01 ^h 33 ^m 46 ^s .3, 30°36'52".0	14.4	42	15.64	0.10	5–6	SSA1472 (SM567)
24	01 ^h 33 ^m 46 ^s .7, 30°36'26".9	14.4	47	18.09	0.10	10–17	...
25	01 ^h 33 ^m 47 ^s .5, 30°39'41".8	11.3	31	18.99	0.10	14–22	SSA1493
26	01 ^h 33 ^m 47 ^s .5, 30°38'36".4	9.0	30	18.23	0.10	7–15	SSA1495
27	01 ^h 33 ^m 48 ^s .1, 30°33'02".3	15.1	51	17.42	0.10	6–12	SSA1499
28	01 ^h 33 ^m 48 ^s .7, 30°38'45".0	8.0	17	19.25	0.10	11–35	SSA1515
29	01 ^h 33 ^m 48 ^s .7, 30°39'30".0	14.0	53	18.06	0.10	5–17	SSA1505 (SM572)
30	01 ^h 33 ^m 49 ^s .1, 30°39'45".3	13.4	59	16.30	0.10	7–8	SSA1516
31	01 ^h 33 ^m 49 ^s .3, 30°38'22".5	12.0	49	17.81	0.10	8–14	...
32	01 ^h 33 ^m 50 ^s .1, 30°37'29".6	9.4	10	18.42	0.10	3–22	SSA1527
33	01 ^h 33 ^m 50 ^s .5, 30°33'46".1	10.0	12	18.95	0.10	15–25	SSA1536
34	01 ^h 33 ^m 51 ^s .2, 30°39'55".8	12.5	73	16.65	0.10	5–7	SSA1550
35	01 ^h 33 ^m 51 ^s .6, 30°37'22".5	10.0	20	19.79	0.10	3–35	...
36	01 ^h 33 ^m 51 ^s .6, 30°38'51".0	12.2	84	17.15	0.10	5–10	SSA1554, SSA1546
37	01 ^h 33 ^m 52 ^s .3, 30°37'56".0	15.1	39	17.93	0.10	8–12	...
38	01 ^h 33 ^m 52 ^s .6, 30°39'20".3	10.0	46	16.42	0.10	3–7	...
39	01 ^h 33 ^m 52 ^s .8, 30°37'15".0	8.6	9	18.14	0.10	3–15	...
40	01 ^h 33 ^m 53 ^s .0, 30°38'59".4	9.5	60	16.91	0.10	3–8	...
41	01 ^h 33 ^m 54 ^s .5, 30°33'04".3	12.2	32	17.17	0.10 ^a	7–11	SSA1586 (SM215, PL167), SSA1598, SSA1585
42	01 ^h 33 ^m 55 ^s .6, 30°37'40".0	10.0	19	18.81	0.10	12–25	SM223
43	01 ^h 33 ^m 56 ^s .7, 30°40'20".0	10.5	15	19.36	0.01	6–35	SM236
44	01 ^h 33 ^m 57 ^s .4, 30°35'30".0	15.0	41	17.68	0.10	12–14	SSA1636 (SM241)
45	01 ^h 33 ^m 57 ^s .9, 30°48'46".2	8.9	11	18.98	0.15 ^a	7–25	PL81
46	01 ^h 33 ^m 58 ^s .6, 30°35'22".5	11.0	41	16.41	0.10	3–7	SSA1647 (SM476)
47	01 ^h 33 ^m 58 ^s .6, 30°48'37".5	10.0	13	18.74	0.10	5–22	SM253
48	01 ^h 33 ^m 59 ^s .0, 30°49'09".2	8.0	10	18.83	0.15 ^a	14–28	SM251 (PL80)
49	01 ^h 33 ^m 59 ^s .1, 30°35'37".5	10.0	32	17.51	0.10	5–12	...
50	01 ^h 33 ^m 59 ^s .1, 30°35'47".2	10.0	28	19.13	0.10	15–19	SSA1654
51	01 ^h 33 ^m 59 ^s .2, 30°40'07".5	20.0	99	18.00	0.10	6–15	SSA1652
52	01 ^h 34 ^m 01 ^s .5, 30°36'20".6	10.8	38	17.61	0.10	6–12	SSA1693
53	01 ^h 34 ^m 01 ^s .6, 30°37'17".0	8.8	20	18.05	0.10	3–15	SSA1700, SSA1682
54	01 ^h 34 ^m 01 ^s .8, 30°46'28".4	16.4	31	18.10	0.10	10–17	SSA1694, SSA1685
55	01 ^h 34 ^m 02 ^s .2, 30°35'56".0	13.2	13	19.21	0.10	3–15	...
56	01 ^h 34 ^m 02 ^s .3, 30°38'40".6	22.4	80	17.03	0.10	5–7	SSA1711 (SM276)
57	01 ^h 34 ^m 02 ^s .6, 30°37'04".5	8.3	9	18.38	0.10	3–15	...
58	01 ^h 34 ^m 03 ^s .2, 30°46'36".7	9.2	9	18.50	0.10	7–19	SSA1715 (SM280)
59	01 ^h 34 ^m 03 ^s .3, 30°36'43".6	9.5	19	18.13	0.10	3–15	...
60	01 ^h 34 ^m 05 ^s .7, 30°47'49".8	10.7	21	17.77	0.20 ^a	3–14	SM297 (PL197)
61	01 ^h 34 ^m 06 ^s .9, 30°47'22".6	13.2	30	16.44	0.20 ^a	3–8	SSA1748 (SM305, PL201)
62	01 ^h 34 ^m 07 ^s .6, 30°39'24".4	16.4	69	18.44	0.10	14–25	...
63	01 ^h 34 ^m 09 ^s .3, 30°39'07".7	14.9	68	16.16	0.10 ^a	3–6	SSA1791, SSA1795, SSA1777 (SM321, PL98), PL97
64	01 ^h 34 ^m 11 ^s .5, 30°36'12".2	17.4	31	17.75	0.10	8–14	SSA1825

Table 3
(Continued)

YSG ID	R.A., Decl. (J2000.0)	r_{cl} ('')	N_{Ostar}	M_v (mag)	$E(B - V)$	Age (Myr)	Cross ID
(1)	(2)	(3)	(4)	(5)	(6)	(7)	(8)
65	01 ^h 34 ^m 14 ^s .0, 30°33'39"7	7.2	16	17.95	0.10	5–15	SSA1862
66	01 ^h 34 ^m 14 ^s .7, 30°33'58"5	10.0	32	17.34	0.10	8–12	...
67	01 ^h 34 ^m 15 ^s .1, 30°33'48"1	7.5	22	18.90	0.10 ^a	3–25	SM478 (PL27)
68	01 ^h 34 ^m 15 ^s .2, 30°35'00"0	8.6	14	17.89	0.10	5–15	SSA1894, SSA1895
69	01 ^h 34 ^m 16 ^s .0, 30°33'37"5	10.0	29	16.66	0.10	3–7	SSA1906 (SM480)
70	01 ^h 34 ^m 16 ^s .8, 30°39'18"0	8.3	10	19.76	0.10	12–50	...
71	01 ^h 34 ^m 31 ^s .4, 30°47'48"0	9.5	11	19.12	0.10	3–28	...
72	01 ^h 34 ^m 33 ^s .0, 30°46'23"8	10.4	21	19.07	0.10	3–28	...
73	01 ^h 34 ^m 33 ^s .4, 30°47'03"5	21.2	169	15.90	0.10	3–5	NGC 604
74	01 ^h 34 ^m 39 ^s .5, 30°41'37"1	8.7	16	18.73	0.10	7–22	SSA2167, SSA2168
75	01 ^h 34 ^m 40 ^s .1, 30°41'56"0	9.2	19	17.69	0.10	3–14	SSA2169, SSA2164

Notes. Column 1: young stellar group (YSG) ID, in order of right ascension. Column 2: central position R.A., decl. of the YSG. Column 3: size of the stellar group, which approximately corresponds to the boundary of $n^* = 2$ stars per area (see Section 3.2.2). Column 4: number of O stars (more massive than O9V-type stars). Column 5: V magnitude of the brightest member in the YSG. Column 6: applied reddening correction for each YSG. Column 7: estimated age of the YSG. Column 8: cross identifications with other catalogs. SM- n : from Sarajedini & Mancone (2007). PL- n : from Park & Lee (2007). SSA- n : from San Roman et al. (2010). NGC- n : giant H II regions.

^a From Chandar et al. (1999), Park & Lee (2007), González Delgado & Pérez (2000), and Churchwell & Goss (1999).

highly obscured regions ($A_{\text{H}\alpha} > 3$ mag) have been found in other nuclei galaxy (Prescott et al. 2007), but we can discard that possibility in M33.

3.4. GMC Types

We classify the GMCs into four types according to the age of the associated YSGs and H II regions.

1. Type A GMCs are not associated with H II regions nor YSGs;
2. Type B GMCs are associated with H II regions, but not with any YSG;
3. Type C GMCs are associated with H II regions and young (<10 Myr) stellar groups; and
4. Type D GMCs are associated with H II regions and relatively old (10–30 Myr) stellar groups.

Note that averaged values between the upper and lower limits of the stellar ages are used for this classification. If a GMC is associated with several YSGs of different ages, the classification is done based on the youngest stellar group.

Table 4 lists the classification of each M33 GMC into one of these four types. Out of the 65 GMCs, 1 (1%), 13 (20%), 29 (45%), and 22 (34%) are found to be Types A, B, C, and D, respectively. Table 5 summarizes these statistics. The Type C GMCs are the majority among all GMC types.

The estimated age of some YSGs may be uncertain. We select 44 GMCs with accurate age estimations for their associated YSGs in order to check how robust the relative percentage is among the different types. In this regard, only YSGs whose age upper limit is smaller than 10 Myr (see Figure 9) and lower limit is larger than 10 Myr (see Figure 10) are used. With this condition, we obtain that 1 (2%), 13 (30%), 19 (43%), and 11 (25%) are classified as Types A, B, C, and D, respectively. The 44 selected GMCs are indicated in Table 4. We confirm the trend in the relative percentages, that Type C GMCs makeup the majority among all GMC types.

A caveat in the Type B and C classifications is that the percentages may be partly influenced by the instrumental sensitivity in Massey et al.’s (2006) survey, which may limit the detection of some YSGs. Given the instrumental sensitivity of

Massey et al.’s (2006) survey, some Type B sources possibly contain YSGs that have not been detected. However, the sensitivity restricts the contained YSGs to be less massive than $13 M_{\odot}$ (\sim B1V star) (Section 3.2.1), and Type C sources (YSGs with ages <10 Myr) are typically more massive than that.

The three GMC classifications in the LMC, Types I, II, and III (Kawamura et al. 2009) correspond to Types A, B, and C in our classification, respectively (see also Table 5). In the LMC, Type II (Type B) represents the largest number among all GMC types, while it is Type C in M33. The percentage of Type C GMCs in M33 (40%–45%) is also larger than in LMC (26%). Note that the clusters with ages of 10–30 Myr in LMC are likely far away from their parent GMCs (Yamaguchi et al. 2001; Kawamura et al. 2009) and thus the relative percentage is largely unknown.

In addition, these discrepancies can be partly explained by the different spatial resolution and observed line, as the classification of LMC GMCs have been done with 40 pc resolution in CO($J = 1-0$) (Fukui et al. 2008). First, the GMCs in M33 are typically double the size of those in LMC. If an M33 GMC is composed of two different types of GMCs, for example Types B and C, whose sizes are comparable to those in the LMC, then the GMC would have been classified as Type C. Therefore, the classifications will be affected. Second, regarding the different tracers used, the M33 GMCs identified from CO($J = 3-2$) data represent the denser and/or warmer molecular gas which is more directly linked to massive SF, while the LMC GMCs identified from CO($J = 1-0$) data trace the bulk of the molecular gas. In fact, in the case of M33 GMCs identified by using CO($J = 1-0$) data, more than two-thirds have associated H II regions (Engargiola et al. 2003), which is of a similar proportion in the LMC (Kawamura et al. 2009).

3.5. Physical Properties of GMC Types

Figure 12 shows the distributions of the line width (ΔV_{FWHM}), deconvolved radius (R_{deconv}), CO($J = 3-2$) luminosity ($L'_{\text{CO}(3-2)}$), averaged line ratio ($R_{3-2/1-0}$), and SFRs of the 65 GMCs. Each row represents each GMC type. The shaded areas represent the histograms for the 44 selected GMCs with more accurate classifications (Section 3.4). Table 6 summarizes

Table 4
Properties of M33 GMCs and Massive Star Formation

GMC ID	Type	YSG ID	$L(\text{H}\alpha)$ (erg s $^{-1}$)	$L(24 \mu\text{m})$ (erg s $^{-1}$)	$A(\text{H}\alpha)$ (mag)	SFR ($M_{\odot} \text{ yr}^{-1}$)	H II Regions/24 μm Source
(1)	(2)	(3)	(4)	(5)	(6)	(7)	(8)
1	C ^a	YSG-72, 73	7.67×10^{39}	4.04×10^{40}	0.20	2.16×10^{-1}	NGC 604
2	D	YSG-45, 47	4.16×10^{37}	6.71×10^{38}	0.52	3.58×10^{-3}	B-005 (V-426), B-074, C-Z233A
3	C ^a	YSG-65, 66, 67, 69	2.59×10^{38}	1.96×10^{39}	0.27	1.05×10^{-2}	C-Z258 (V-115), B-066
4	D	YSG-64	3.80×10^{38}	1.63×10^{39}	0.16	8.73×10^{-3}	B-709 (V-174), C-Z407 (V-195)
5	C ^a	YSG-38, 40	3.48×10^{38}	1.51×10^{39}	0.17	8.09×10^{-3}	C-Z160A (V-84)
6	D ^a	YSG-5	1.40×10^{37}	2.13×10^{39}	2.08	1.13×10^{-2}	B-033, B-628, B-203 (V-280, V-273), H-634 (V-234)
7	C ^a	YSG-2	2.89×10^{39}	1.42×10^{40}	0.19	7.60×10^{-2}	NGC 595 (V-184)
8	B ^a	...	2.17×10^{36}	9.04×10^{37}	1.03	4.81×10^{-4}	C-Z322, C-Z324, B-647 (V-434), B-302 (V507), V-407
9	C	YSG-7, 9	8.54×10^{37}	4.76×10^{38}	0.21	2.55×10^{-3}	C-Z112, C-Z214, V-168
10	C ^a	YSG-22	6.94×10^{37}	4.07×10^{38}	0.22	2.18×10^{-3}	C-Z219 (V-65), B-641, B-633
11	D ^a	YSG-33	1.16×10^{38}	1.47×10^{38}	0.05	8.01×10^{-4}	B-047, B-014 (V-131)
12	C ^a	YSG-62, 63	5.06×10^{37}	3.94×10^{38}	0.28	2.10×10^{-3}	B-689 (V-266), B-702 (V-240), C-Z251 (V-271)
13	C	YSG-1	2.47×10^{38}	2.13×10^{39}	0.31	1.14×10^{-2}	B-211, C-Z109, C-Z045 (V-70)
14	C ^a	YSG-60, 61	5.83×10^{38}	2.01×10^{39}	0.13	1.08×10^{-2}	B-690, C-Z183, C-Z249
15	C ^a	YSG-18	1.10×10^{36}	1.89×10^{38}	2.19	1.01×10^{-3}	C-Z010A, B-044, B-038 (V-210)
16	D ^a	YSG-45, 48	4.04×10^{37}	1.66×10^{38}	0.16	8.90×10^{-4}	B-703 (V-431), B-669 (V-427), B-696 (V-429), C-224
17	C ^a	YSG-56	2.49×10^{37}	1.62×10^{38}	0.24	8.66×10^{-4}	C-Z405 (V-198)
18	C ^b	YSG-44, 46, 49, 50	2.19×10^{38}	2.55×10^{39}	0.40	1.36×10^{-2}	C-Z001A (V-165), V-199
19	D ^a	YSG-4	1.95×10^{38}	1.05×10^{39}	0.20	5.62×10^{-3}	B-251 (V-193)
20	C ^a	YSG-56	3.80×10^{38}	1.63×10^{39}	0.16	8.73×10^{-3}	C-Z405 (V-198)
21	D ^a	YSG-42	1.47×10^{37}	1.89×10^{38}	0.43	1.01×10^{-3}	IC142
22	D ^a	YSG-70	1.61×10^{37}	3.83×10^{38}	0.70	2.04×10^{-3}	C-Z274
23	C ^a	YSG-21, 23, 24	2.19×10^{38}	1.14×10^{39}	0.20	6.10×10^{-3}	B-1002, B-060 (V-185), V-223
24	C	YSG-27	1.99×10^{38}	1.07×10^{39}	0.20	5.73×10^{-3}	B-631 (V-127), B-019, V-113
25	C	YSG-52, 53, 57, 59	7.26×10^{37}	6.94×10^{37}	0.04	3.81×10^{-4}	B-672, C-Z245
26	D	YSG-68	9.78×10^{37}	6.72×10^{38}	0.25	3.59×10^{-3}	C-Z322A (V-47), B-660, C-Z172
27	D	YSG-72	7.27×10^{38}	1.64×10^{39}	0.09	8.84×10^{-3}	NGC 604
28	D ^b	YSG-43, 51	3.10×10^{36}	9.60×10^{37}	0.84	5.11×10^{-4}	H-744, H-731 H-740
29	C ^a	YSG-30, 34	1.23×10^{38}	3.42×10^{38}	0.11	1.84×10^{-3}	C-Z150, B-064, C-Z144 (V-72)
30	C	YSG-3	1.46×10^{38}	1.19×10^{39}	0.29	6.35×10^{-3}	C-Z210 (V-60)
31	D ^a	YSG-26, 28, 31	2.35×10^{38}	7.03×10^{38}	0.12	3.78×10^{-3}	B-017 (V-239)
32	D	YSG-32, 35	1.07×10^{38}	8.91×10^{38}	0.30	4.76×10^{-3}	B-020 (V-201), B-637
33	C ^a	YSG-18	1.54×10^{38}	7.35×10^{38}	0.18	3.94×10^{-3}	B-038 (V-210)
34	D	YSG-71	1.04×10^{39}	2.15×10^{39}	0.08	1.16×10^{-2}	NGC 604, B-652
35	B ^a	...	6.04×10^{37}	4.35×10^{37}	0.03	2.41×10^{-4}	C-Z347, C-Z353
36	D	YSG-54, 58	6.17×10^{37}	2.22×10^{38}	0.14	1.19×10^{-3}	C-Z291, B-081
37	C	YSG-16, 17, 20	1.31×10^{38}	5.76×10^{38}	0.17	3.09×10^{-3}	B-061, C-Z139, C-Z010
38	D	YSG-12	2.04×10^{38}	9.55×10^{38}	0.18	5.11×10^{-3}	B-612, B-058 (V-144), C-Z135, C-Z081
39	C	YSG-3	2.77×10^{37}	1.19×10^{39}	1.05	6.34×10^{-3}	C-Z210 (V-60), B-034
40	D	YSG-8, 10, 11, 13	2.07×10^{37}	2.56×10^{38}	0.42	1.37×10^{-3}	B-200, B-206
41	C ^a	YSG-36, 38, 40	2.18×10^{38}	9.18×10^{37}	0.02	5.24×10^{-4}	C-Z160A (V-84), B-010
42	C ^a	YSG-25, 29, 30	9.66×10^{37}	1.29×10^{39}	0.45	6.88×10^{-3}	C-Z144 (V-72), B-037, C-Z221, B-066
43	C	YSG-41	3.11×10^{38}	1.24×10^{39}	0.15	6.65×10^{-3}	B-092 (V-97)
44	C	YSG-39	6.61×10^{36}	3.35×10^{37}	0.19	1.79×10^{-4}	C-Z227
45	D	YSG-35, 37	1.01×10^{37}	7.23×10^{37}	0.26	3.86×10^{-4}	B-1501
46	D ^a	YSG-15	3.28×10^{36}	7.27×10^{37}	0.66	3.87×10^{-4}	H-601, H-598 (V-283)
47	C ^b	YSG-55	2.19×10^{38}	7.03×10^{37}	0.01	4.10×10^{-4}	C-Z246A (V-122)
48	B ^a	...	2.77×10^{36}	2.59×10^{37}	0.33	1.38×10^{-4}	H-1145 (V-277), H-1146, H-1266 (V-281)
49	D	YSG-13	1.21×10^{38}	3.54×10^{38}	0.11	1.90×10^{-3}	B-050 (V-91)
50	D ^a	YSG-6	5.80×10^{37}	1.36×10^{38}	0.09	7.33×10^{-4}	NGC 595
51	B ^b	...	6.06×10^{37}	7.85×10^{37}	0.05	4.28×10^{-4}	B-209, B-610, V-182
52	C ^a	YSG-62, 63	5.73×10^{37}	1.54×10^{38}	0.11	8.29×10^{-4}	C-Z182, B-689 (V-266)
53	B ^a	...	3.89×10^{37}	2.63×10^{38}	0.25	1.41×10^{-3}	C-Z041 (V-69)
54	B ^a	...	4.12×10^{37}	1.48×10^{38}	0.14	7.94×10^{-4}	B-665 (V-438), V-398, V-407
55	B ^a	...	9.58×10^{37}	6.81×10^{37}	0.03	3.78×10^{-4}	B-302 (V-507), V-420
56	C ^a	YSG-18	1.54×10^{38}	7.35×10^{38}	0.18	3.94×10^{-3}	B-038 (V-210), B-051
57	B ^a	...	8.55×10^{36}	3.89×10^{37}	0.17	2.08×10^{-4}	C-Z212 (V-422), H-769 (V-385)
58	B ^b	...	6.26×10^{36}	2.50×10^{37}	0.15	1.34×10^{-4}	C-Z146 (V-209)
59	D ^a	YSG-20	5.53×10^{37}	1.26×10^{38}	0.09	6.79×10^{-4}	B-021, C-Z220, B-636
60	A ^a	...	3.81×10^{35}	1.67×10^{37}	1.06	8.89×10^{-5}	
61	C ^a	YSG-12, 14	1.81×10^{38}	9.55×10^{38}	0.20	5.11×10^{-3}	B-612, B-058 (V-144)
62	B ^a	...	1.09×10^{37}	8.03×10^{37}	0.27	4.29×10^{-4}	C-Z299 (V-402)
63	C	YSG-74, 75	2.68×10^{38}	9.17×10^{38}	0.13	4.92×10^{-3}	B-0654, B0738
64	D ^a	YSG-33	1.02×10^{38}	1.47×10^{38}	0.06	7.99×10^{-4}	B-014 (V-131)

Table 4
(Continued)

GMC ID (1)	Type (2)	YSG ID (3)	$L(\text{H}\alpha)$ (erg s $^{-1}$) (4)	$L(24 \mu\text{m})$ (erg s $^{-1}$) (5)	$A(\text{H}\alpha)$ (mag) (6)	SFR ($M_{\odot} \text{ yr}^{-1}$) (7)	H II Regions/24 μm Source (8)
65	B ^a	...	1.94×10^{37}	7.66×10^{37}	0.15	4.11×10^{-4}	C-Z242 (V-486)
66	B ^a	...	5.25×10^{36}	2.95×10^{37}	0.21	1.58×10^{-4}	H-931, H945, H-944, H-939
67	C ^a	YSG-19	9.20×10^{36}	1.30×10^{38}	0.47	6.93×10^{-4}	B-614, V-100
68	B ^a	...	2.49×10^{35}	4.65×10^{37}	2.27	2.47×10^{-4}	H-907, H-933
69	B ^a	...	5.50×10^{35}	2.82×10^{37}	1.17	1.50×10^{-4}	H-823, V-502
70	B ^a	...	3.08×10^{37}	2.52×10^{38}	0.29	1.35×10^{-3}	H-793, V-227
71	B ^b	...	1.59×10^{37}	8.05×10^{37}	0.19	4.31×10^{-4}	C-Z040

Notes. Column 1: GMC ID. Column 2: GMC classifications: Type A shows no signature of massive star formation; Type B is associated with H II region(s); Type C is associated with H II region(s) and less than 10 Myr old stellar group(s); and Type D is associated with H II region(s) and 10–30 Myr old stellar group(s). Column 3: young stellar groups (YSGs) associated with the GMCs. Column 4: luminosity of H α , as measured over the extent of a GMC. Column 5: luminosity of 24 μm , as measured over the extent of a GMC. Column 6: the H α attenuation is calculated as $A_{\text{H}\alpha} = 2.5 \log[1 + 0.038 L(24 \mu\text{m})/L(\text{H}\alpha)]$ (Calzetti et al. 2005; Prescott et al. 2007). Column 7: star formation rate (SFR), derived from $L(24 \mu\text{m})$ and $L(\text{H}\alpha)$ using the relation between the extinction-corrected H α line emission and the SFR in Calzetti et al. (2007). Column 8: name of the associated H II regions : B-n from Boulesteix et al. (1974); C-n from Courtes et al. (1987); H-n from Hodge et al. (1999); V-n from Verley et al. (2007). The names within parenthesis indicate a counterpart of H II regions in the 24 μm catalog.

^a The selected GMCs with more accurate classification. See details in the text in Section 3.4.

^b GMCs at the edge of the fields of view. The values just provide lower limits.

Table 5
GMC Classification and Evolution

GMC Type	Observed Signature	Number of GMCs	LMC ^a
A	No H II regions or young stellar groups	1 (1%)	46 (24%)
B	With H II region(s), but no young stellar groups	13 (20%)	96 (50%)
C	With H II region(s) and young (<10-Myr) stellar group(s)	29 (45%)	49 (26%)
D	With H II region(s) and relatively old (>10-Myr) stellar group(s)	22 (34%)	...

Note. ^a GMC Type in LMC (Kawamura et al. 2009). The definition of Types A, B, and C in our classification correspond to their Types I, II, and III, respectively.

the mean and standard deviation of these variables for each GMC type. The $R_{3-2/1-0}$ distributions of Types C and D show a peak over 0.4, while those of Type B are always smaller than the average value of the former types (i.e., $R_{3-2/1-0} < 0.3$). The SFR distributions of Types C and D show a peak over $2 \times 10^{-2} M_{\odot} \text{ yr}^{-1}$, while those of the other three types are smaller. We have used Kolmogorov-Smirnov (K-S) tests to check whether the distributions for the different types differ. We cannot discard that the ΔV_{FWHM} , R_{deconv} , and $L'_{\text{CO}(3-2)}$ distributions for these three types arise from the same distribution. However, the test indicates that $R_{3-2/1-0}$ and SFR distributions of Types C and D are different from those of Type B (p -value < 0.01). The selected GMCs with more accurate classification, as shown in the shaded histograms (Figure 12), indicate that the average values of all quantities for Type C are the largest, followed by Type D, Type B, and Type A, in that order. This suggests that the Type C GMCs are relatively large and show the most active SF among all types. Note that all quantities of the single Type A object are smaller than for the other three types. However, additional Type A sources need to be identified to properly characterize the properties of this class of objects.

In the following subsections, we present a close-up view of the CO($J = 3-2$), CO($J = 1-0$), $R_{3-2/1-0}$, and H α maps of the largest GMC in each GMC type, in order to illustrate the different properties among the four GMC types. Figures 13–16 show for four GMCs representative of each type: (a) the CO($J = 3-2$) integrated intensity map, (b) CO($J = 1-0$) map, (c) the $R_{3-2/1-0}$ map, and (d) the H α images. GMC-60 is chosen as a representative of Type A, GMC-8 of Type B, GMC-1 of

Type C, and GMC-16 of Type D. The positions of H II regions, the 24 μm sources, and the surface density map of young stars are also marked in these figures.

The CO($J = 3-2$) emission peaks are in general slightly offset from the CO($J = 1-0$) emission peak as we mentioned in Section 3.1.1, but they are closer to the location of massive SF sites such as YSGs and H II regions. These differences of spatial distributions necessarily result in a relatively high $R_{3-2/1-0}$ area in a GMC around such massive SF sites, and a gradient of $R_{3-2/1-0}$ that gradually increases in the direction toward such massive SF sites.

3.5.1. GMCs without Massive SF Regions (Type A)

Figure 13 shows the images of GMC-60 of Type A. No large variations in $R_{3-2/1-0}$ (~ 0.28 on average over the GMC) or bright H α emission spots in this GMC are found. In addition, it is a relatively small GMC compared to the average size and mass of all identified GMCs (Table 6). Since only one GMC is classified as Type A, it is unclear whether the Type A source is representative of a class of similar sources or just a statistical outlier. Additional Type A sources need to be identified to properly characterize the properties of this class of objects.

3.5.2. GMCs with H II Regions but Not YSGs (Type B)

One-fifth of the GMCs in our catalog are classified as Type B. We cannot assure significant differences in ΔV_{FWHM} , size, and $L'_{\text{CO}(3-2)}$ compared to those of Type C and Type D (see Figure 12). However, the $R_{3-2/1-0}$ is smaller than the latter two

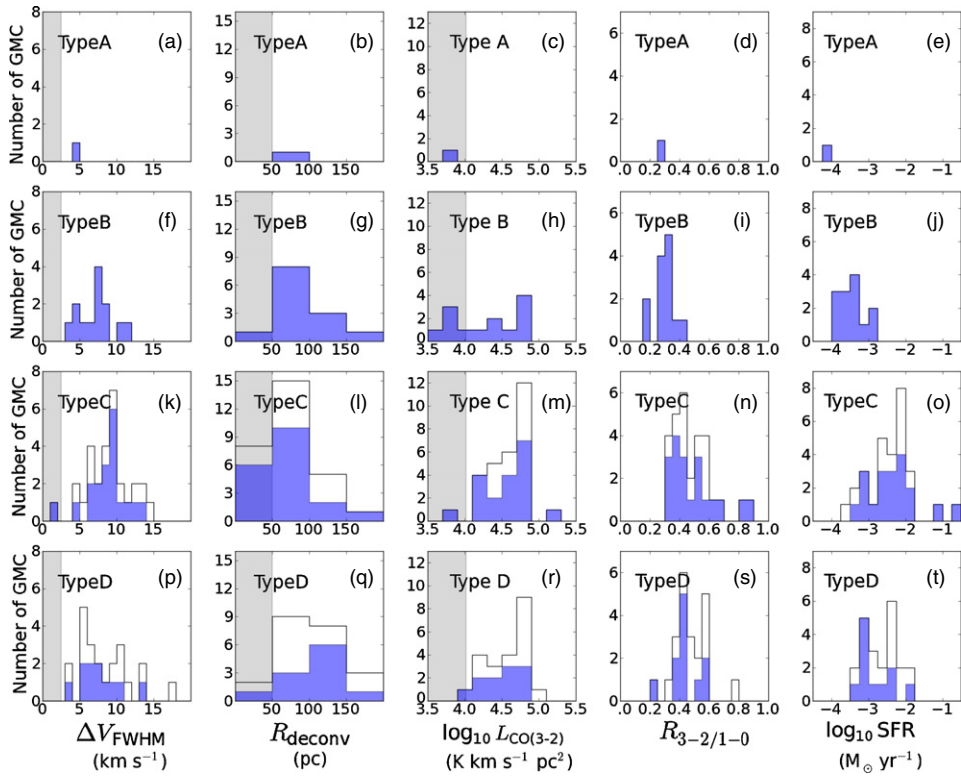


Figure 12. Histograms of ΔV_{FWHM} , R_{deconv} , $L'_{\text{CO(3-2)}}$, $R_{3-2/1-0}$, and SFRs for the 65 GMCs. Panels (a)–(d), (f)–(j), (k)–(o), and (p)–(t) show the properties of GMC Type A, Type B, Type C, and Type D, respectively. The shaded areas indicate the detection limits: $\Delta V_{\text{FWHM}} = 2.5 \text{ km s}^{-1}$, $R_{\text{deconv}} = 50 \text{ pc}$, and $L'_{\text{CO(3-2)}} = 10^4 \text{ K km s}^{-1} \text{ pc}^2$. Note that R_{deconv} is not derived for 31 GMCs because the size cannot be derived for those with a minor axis less than the beam size, and thus we set the non-deconvolved radius as the upper limit. The (blue) filled histogram indicates the selected 44 GMCs that are associated with the YSGs with confirmed ages (see details in Section 3.4).

(A color version of this figure is available in the online journal.)

Table 6
Physical Properties of the GMC Types

GMC	Line Width		Size		Luminosity		Ratio		SFR		
	Type	$\langle \Delta V \rangle$	$\sigma_{\Delta V}$	$\langle R_{\text{deconv}} \rangle$	$\sigma_{R_{\text{deconv}}}$	$\langle L'_{\text{CO(3-2)}} \rangle$	$\sigma_{L'_{\text{CO(3-2)}}}$	$\langle R_{3-2/1-0} \rangle$	$\sigma_{R_{3-2/1-0}}$	$\langle \text{SFR} \rangle$	σ_{SFR}
		(km s $^{-1}$)	(km s $^{-1}$)	(pc)	(pc)	($10^4 \text{ K km s}^{-1} \text{ pc}^2$)	($10^4 \text{ K km s}^{-1} \text{ pc}^2$)			($10^{-3} M_{\odot} \text{ yr}^{-1}$)	
A ^a	4.6	...	<86 ^b	...	0.8	...	0.28	...	0.09	...	
B	7.2	2.2	69 ^b	36	2.8	2.1	0.30	0.07	0.51	0.43	
C	8.8	3.0	64 ^b	38	4.4	2.8	0.49	0.14	14.26	40.42	
D	8.4	3.5	83 ^b	37	4.4	2.3	0.47	0.11	3.60	3.49	
Selected ^c											
A ^a	4.6	...	<86 ^b	...	0.8	...	0.28	...	0.09	...	
B	7.2	2.2	69 ^b	36	2.8	2.1	0.30	0.07	0.51	0.43	
C	8.6	2.8	69 ^b	36	4.4	3.3	0.49	0.16	19.27	49.15	
D	7.6	2.7	103 ^b	32	3.9	2.1	0.43	0.09	2.55	3.17	

Notes.

^a The values for the single GMC classified as Type A (GMC-60) are presented for reference.

^b When the minor axis of a GMC is smaller than the beam size, the deconvolved radius cannot be derived, and then the non-deconvolved radius is used as an upper limit.

^c When only GMCs with more accurate classifications are used (44 GMCs), 1 (2%), 13 (30%), 19 (43%), and 11 (25%) are classified as Types A, B, C, and D, respectively. See details in Section 3.4.

types, with $R_{3-2/1-0} \sim 0.3$ on average and never exceeding 0.5. In addition, the SFR is also lower than the latter two types. We find that all Type B GMCs share a common trend, in the sense that higher $R_{3-2/1-0}$ inside GMCs are preferentially found close to H II regions and 24 μm sources, although the peak of $R_{3-2/1-0}$ is not always coincident with the central position of H II regions. No large spatial variation in $R_{3-2/1-0}$ over the GMC is found.

The associated H II regions and 24 μm sources show a relatively random distribution over the GMC. In addition, these sources are relatively small both in extent and in luminosity. In fact, we find that they do not usually exceed $L(\text{H}\alpha) \sim 10^{38} \text{ erg s}^{-1}$ or $L(24 \mu\text{m}) \sim 10^{38.5} \text{ erg s}^{-1}$, which corresponds to a single O7.5V star (Martins et al. 2005), assuming the conversion factor from ionizing photon rates and extinction-corrected

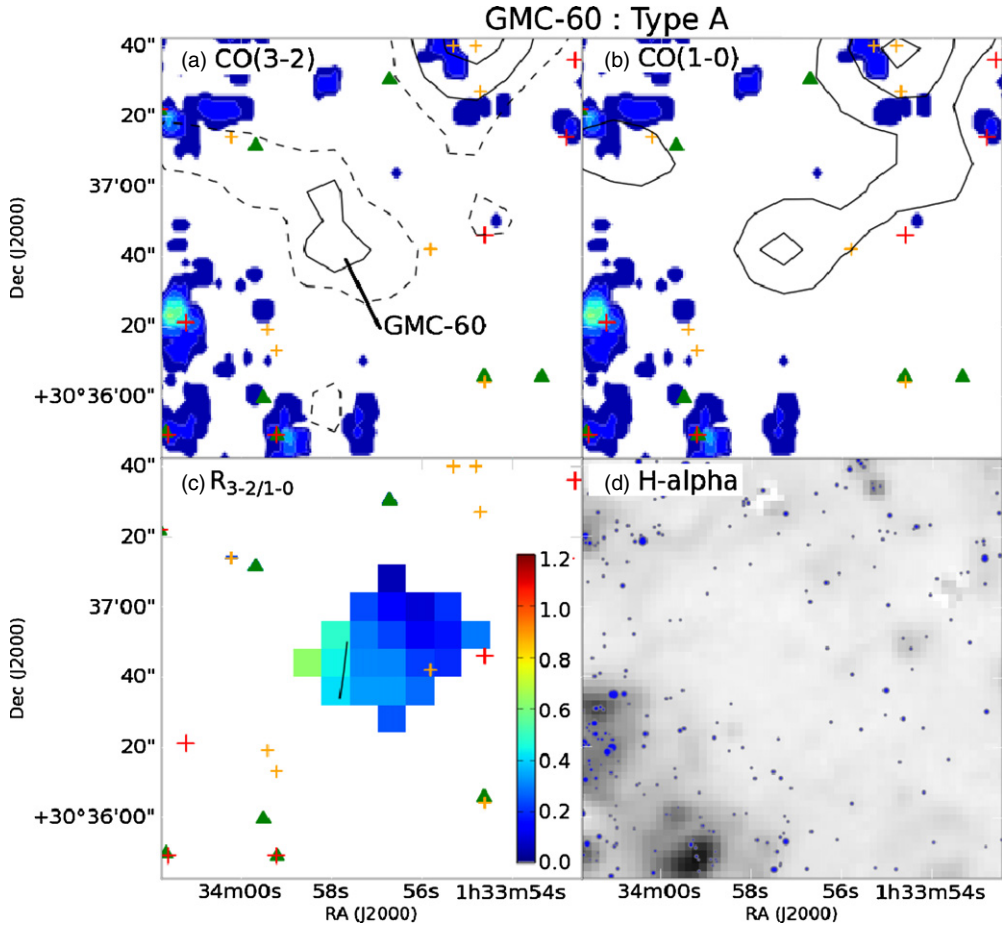


Figure 13. Distribution of (a) $\text{CO}(J = 3-2)$ and (b) $\text{CO}(J = 1-0)$ emission for the single Type A GMC identified in M33, GMC-60, overlaid on the surface density map of young stars (same as Figure 5). The integrated velocity ranges from $V_{\text{LSR}} = -171$ to -161 km s^{-1} . Contour levels are 1, 2, 3, ..., 20 K km s^{-1} . Dashed contours indicate 0.5 K km s^{-1} level. Note that the contour levels below 2 K km s^{-1} are not shown for the $\text{CO}(J = 1-0)$ map. The red and orange crosses, and green triangles are the same as in Figure 7. (c) The $R_{3-2/1-0}$ map for GMC-60. Contour levels are 0.4, 0.6, 0.8, and 1.0. The color range spans from 0 to 1.2, and is shown on the right side of the panel. (d) The distribution of $\text{H}\alpha$ emission around GMC-60. The blue circles represent young stars which are selected using our criteria (Figure 4(a)). Their sizes are proportional to the stellar brightness in the V band.

$\text{H}\alpha$ luminosities in Mayya & Prabhu (1996). This suggests that the associated $\text{H}\alpha$ regions are ionized primarily by a star as massive as a O7.5V star or a later type of OB stars accompanied by several other less massive stars.

As an example of Type B GMCs, we present a close-up view of GMC-8 in Figure 14. This GMC is known as the most massive GMC as traced by $\text{CO}(J = 1-0)$ (Engargiola et al. 2003; Rosolowsky et al. 2007), but it is just identified in our $\text{CO}(J = 3-2)$ catalog as the eighth brightest GMC. The $\text{CO}(J = 3-2)$ emission shows a more compact distribution than that of $\text{CO}(J = 1-0)$ and the emission peaks coincide. The $R_{3-2/1-0}$ slightly increases at the center of the GMC or close to $\text{H}\alpha$ regions and $24 \mu\text{m}$ sources, but no large variation is found over the entire GMC.

3.5.3. GMCs with $\text{H}\alpha$ Regions and YSGs (Type C)

About half of the GMCs in our catalog are classified as Type C. The ΔV_{FWHM} , size, and $L'_{\text{CO}(3-2)}$ of this type are similar to those in other types, but $R_{3-2/1-0}$ and SFRs are the largest among all of them (Figure 12 and Table 6). There are gradients of $R_{3-2/1-0}$ around massive SF sites. Peaks of $R_{3-2/1-0}$ do not coincide in general with the positions of these SF sites, as also found in Type B GMCs. The average $R_{3-2/1-0}$ of this type, ~ 0.5 , is usually larger than that of Type B, and even exceeds over 1.0 at its peak. In addition, unlike Type B, we find that the

associated $\text{H}\alpha$ regions usually exceed the equivalent $L(\text{H}\alpha)$ of a single O7.5 star.

As an example of Type C GMCs, we show the maps for GMC-1 in Figure 15. The $\text{CO}(J = 3-2)$ emission shows a more compact distribution than that of $\text{CO}(J = 1-0)$. GMC-1 overlaps with two YSGs, YSG-73 (corresponding to the GHR NGC 604) and YSG-72. The emission peak of $\text{CO}(J = 3-2)$ is offset from that of $\text{CO}(J = 1-0)$ and is located northward, closer to the largest YSG, YSG-73, and the center of the GHR. A high $R_{3-2/1-0} (> 0.8)$ area is found on the southern side of YSG-73, where compact $\text{H}\alpha$ regions are located (Churchwell & Goss 1999; Tosaki et al. 2007). High $R_{3-2/1-0} (> 0.8)$ preferentially around the GRs suggests that these areas may be excited by young massive stars (Tosaki et al. 2007). A gradient of $R_{3-2/1-0}$ extends from its peak to the south. Panel (d) shows that the concentrations of many bright (massive) stars are located at the heart of the GHR. Note that it is not certain whether or not the YSG-72 is physically associated with this GMC and NGC 604 because there is no spatial correlation between the YSG, $\text{H}\alpha$ region, and $R_{3-2/1-0}$.

3.5.4. GMCs with $\text{H}\alpha$ Regions and 10–30 Myr YSGs (Type D)

About one-third of the GMCs in our catalog are classified as Type D. Generally, the physical properties of this type are similar to Type C (see Figure 12 and Table 6). We also find that

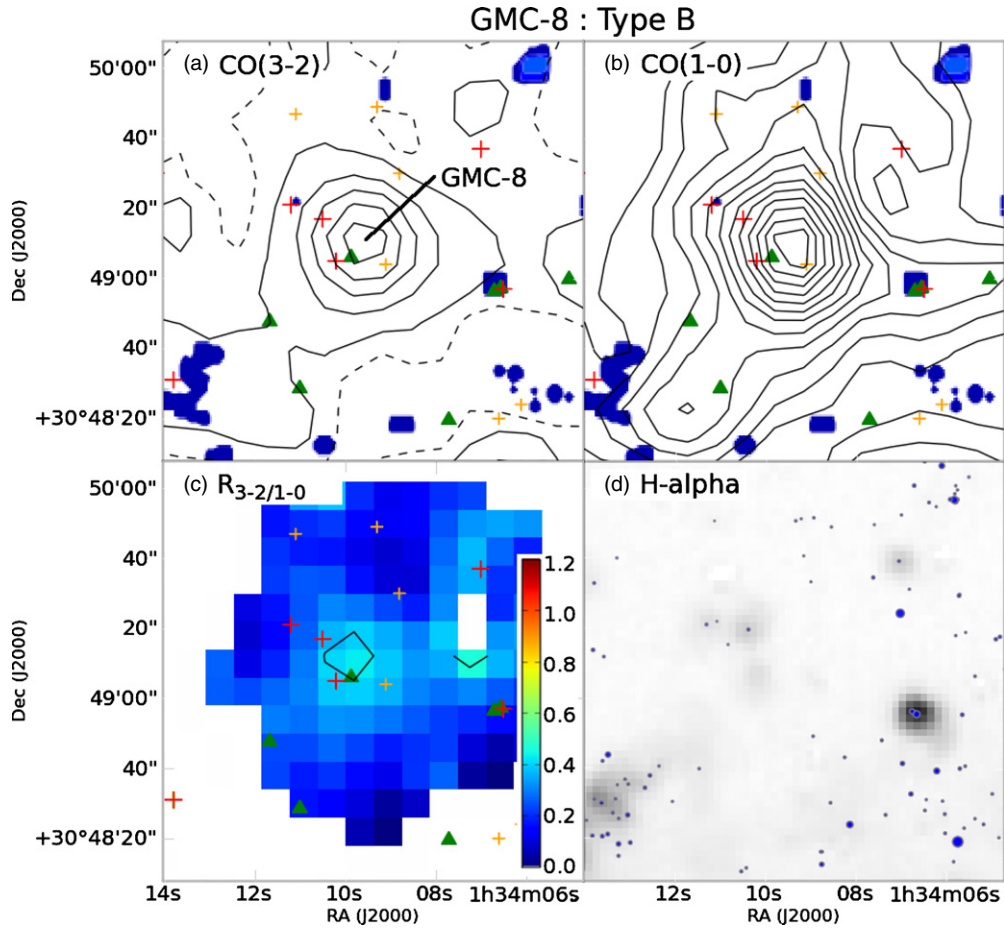


Figure 14. Same as Figure 13, but for GMC-8 representing Type B. The integrated velocity range used in the moment maps is $V_{\text{LSR}} = -264$ to -239 km s^{-1} .

the associated H II regions are slightly less bright than those in Type C, but larger than those in Type B.

Figure 16 shows the maps of GMC-16, a representative of Type D GMCs. The CO($J = 3-2$) emission shows a similar distribution to CO($J = 1-0$), and both CO peaks coincide. Again, the peak of $R_{3-2/1-0}$ (~ 0.4 – 0.6) is preferentially enhanced in the vicinity of the associated massive SF sites but not always coincident with them. Such relatively high $R_{3-2/1-0}$ area is elongated from north to south and there is a gradient of $R_{3-2/1-0}$ from the $R_{3-2/1-0}$ peak in the middle of the GMC to the both west and east edges of the GMC.

4. DISCUSSION

4.1. Evolution of the GMCs

In this section, we discuss based on our results the possible evolution of a GMC by focusing on the dense gas formation occurring around the first generated stars, which presumably leads to SF. We also estimate the typical lifetime of a GMC in M33.

Since there is no correlation between H II regions or YSGs, we infer that Type A is at an evolutionary stage before massive SF. In the case of LMC with 40 pc resolution and using the CO($J = 1-0$) line (Fukui et al. 2008), Kawamura et al. (2009) have shown that about a quarter of all GMCs are Type A. Possible reasons that so few GMCs in M33 are classified as Type A are spatial resolution and sensitivity limit and the choice of the molecular gas tracer, as explained in Section 3.4. Type

B GMCs, which are associated with H II regions but not with YSGs, are interpreted as being at an evolutionary stage just after the formation of massive stars, such as a single O7.5V star or later OB-type stars, that are still partly embedded in the optical as YSGs. We suggest that Type C GMCs being associated both with H II regions and very YSGs (less than 10 Myr) are at an evolutionary stage with active massive SF, as massive as earlier types of O7.5V stars. Type D GMCs associated with H II regions and relatively old (10–30 Myr) stellar groups are considered to be at an evolutionary stage where they have been continuously forming massive stars for over at least 10 Myr.

We find that $R_{3-2/1-0}$ is enhanced around the massive SF sites for Types B, C, and D GMCs (Sections 3.5.2–3.5.4). In order to roughly quantify the offset between them, we plot in Figure 17 the number of pixels above a certain $R_{3-2/1-0}$ (0.1, 0.3, 0.5, 0.7, and 0.9) as a function of the distance to its closest YSG. The average sizes of the 75 YSGs are shown in the same figure, for reference. The dashed lines represent the frequency distribution expected if the same number of YSGs are distributed at random in the observed area. This shows that the distance to the nearest YSG becomes smaller as $R_{3-2/1-0}$ increases, but it must be noted that the $R_{3-2/1-0}$ peaks and the nearest YSGs do not coincide in general.

We can assume that $R_{3-2/1-0}$ is a good tracer of density when $R_{3-2/1-0} < 0.7$, if kinetic temperature is low ($\sim 20 \text{ K}$), as explained in Muraoka et al. (2007). This suggests that the dense molecular gas fraction is enhanced in the vicinity of

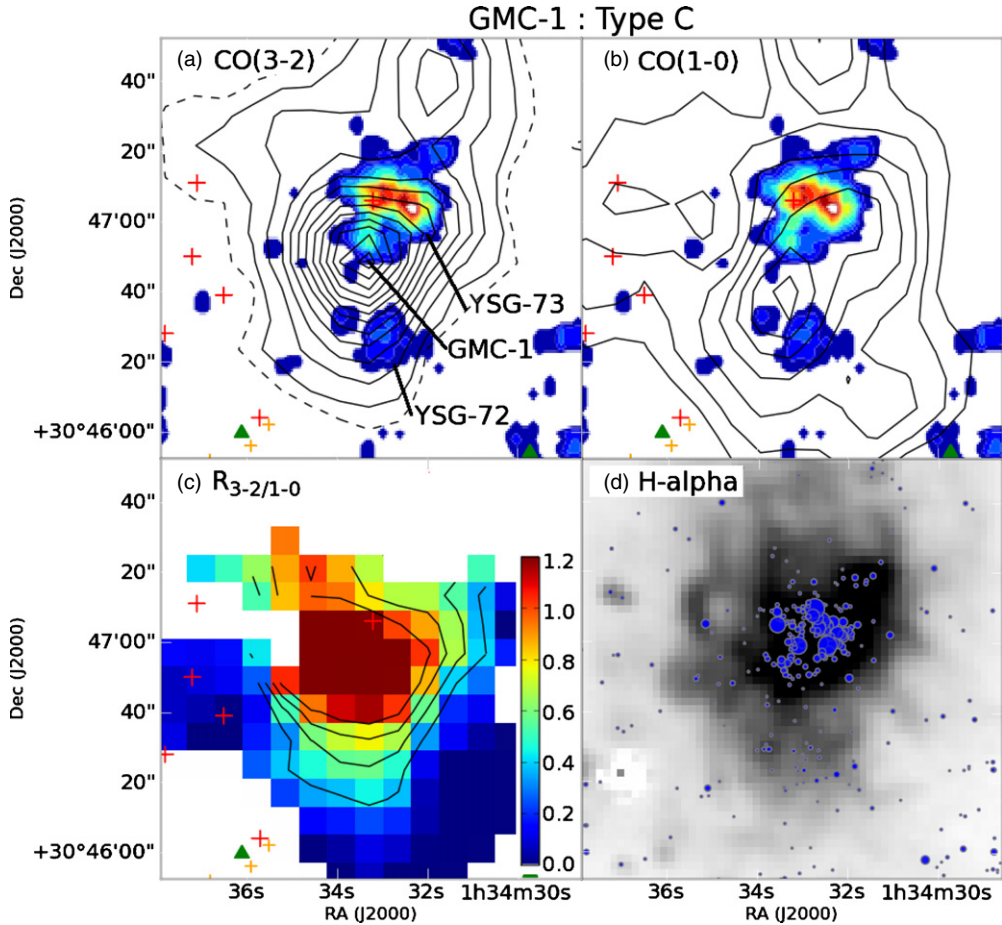


Figure 15. Same as Figure 13, but for GMC-1 representing Type C. The integrated velocity range used in the moment maps is $V_{\text{LSR}} = -259$ to -229 km s^{-1} .

previously formed YSGs. For regions with high $R_{3-2/1-0} > 0.8$, the molecular gas can have a higher kinetic temperature due to the nearest GHRs and YSGs (within ~ 50 pc). This is in good agreement with the suggestion by Wilson et al. (1997) that the GHRs may raise the kinetic temperature of the neighboring (< 100 pc) molecular gas. Therefore, the enhancement of the dense molecular gas fraction around the previously formed massive stars implies that once SF starts, dense gas formation is favored around the SF sites, which will then lead to the next generation of SF.

Next we estimate a lower limit of the lifetime of a GMC from the age of the oldest stellar group contained within the GMC, assuming that the GMCs and YSGs are being formed in a nearly steady evolution. If the classification is done based on the oldest stellar group within a GMC, the frequency distribution of each type is 1 (2%), 13 (20%), 19 (29%), and 32 (49%) out of 65 selected GMCs. The YSGs associated with Type C and Type D GMCs are 8 ± 4 Myr and 18 ± 10 Myr old on average, respectively. Therefore, we estimate that the timescale for each evolutionary stage is 8 ± 4 and 10 ± 6 Myr in Type C and Type D, from the age difference between the associated YSGs. If we further assume that the timescale for each evolutionary stage is proportional to the number of GMCs, then Types A, B, C, and D are estimated to be ~ 1 , 3–7, 5–10, and 8–17 Myr, respectively. As a result, the typical lifetime (from Type A to Type D) of a GMC with masses of $\gtrsim 10^5 M_\odot$ is roughly 20–40 Myr. Note that these results do not change significantly when we use only 44 GMCs with accurate ages for their YSGs (Section 3.4).

In LMC, the lifetime of a GMC with mass as small as $5 \times 10^4 M_\odot$ was estimated to be 20–30 Myr (Fukui et al. 1999; Yamaguchi et al. 2001; Kawamura et al. 2009). The timescales of Types A, B, and C in LMC (corresponding to Types I, II, and III) are 6 Myr, 13 Myr, and 7 Myr, respectively. The timescales for Type B in M33 are smaller than that in LMC, and for Type C they are similar or slightly larger. It is not appropriate to compare the lifetime for Type A in M33 and in LMC because of the limited number of GMCs in this type. No classification exists for LMC GMCs after Type C, and thus we cannot compare them (see Section 3.4 for a discussion). Taking into account that M33 GMCs are a few times larger than the LMC GMCs, M33 Type C and D GMCs are possibly composed of smaller clouds. If that is the case, these small clouds in M33 Types C and D may not be coeval. This can explain the fact that the timescale of Type C GMCs in M33 are slightly larger than in LMC.

In conclusion, we propose a scenario as follows. First, dense gas formation occurs at a certain place in a GMC. After the molecular gas become dense enough to form stars (Type A), massive SF occurs in such dense regions, forming H α regions (Type B). About 4–8 Myr later, the first formed YSGs are not embedded anymore and become visible (Type C). Subsequent dense molecular gas formation occurs due to the effect of previously formed YSGs and the next-generation stars are born in such a dense gas (Type D). In this way, the SF propagates from initially generated stars, until the reservoir of molecular gas is exhausted. Such a continuous SF can last at least 10–30 Myr in a GMC with a typical mass of $\gtrsim 10^5 M_\odot$ during their lifetime of 20–40 Myr (after the dense gas formation).

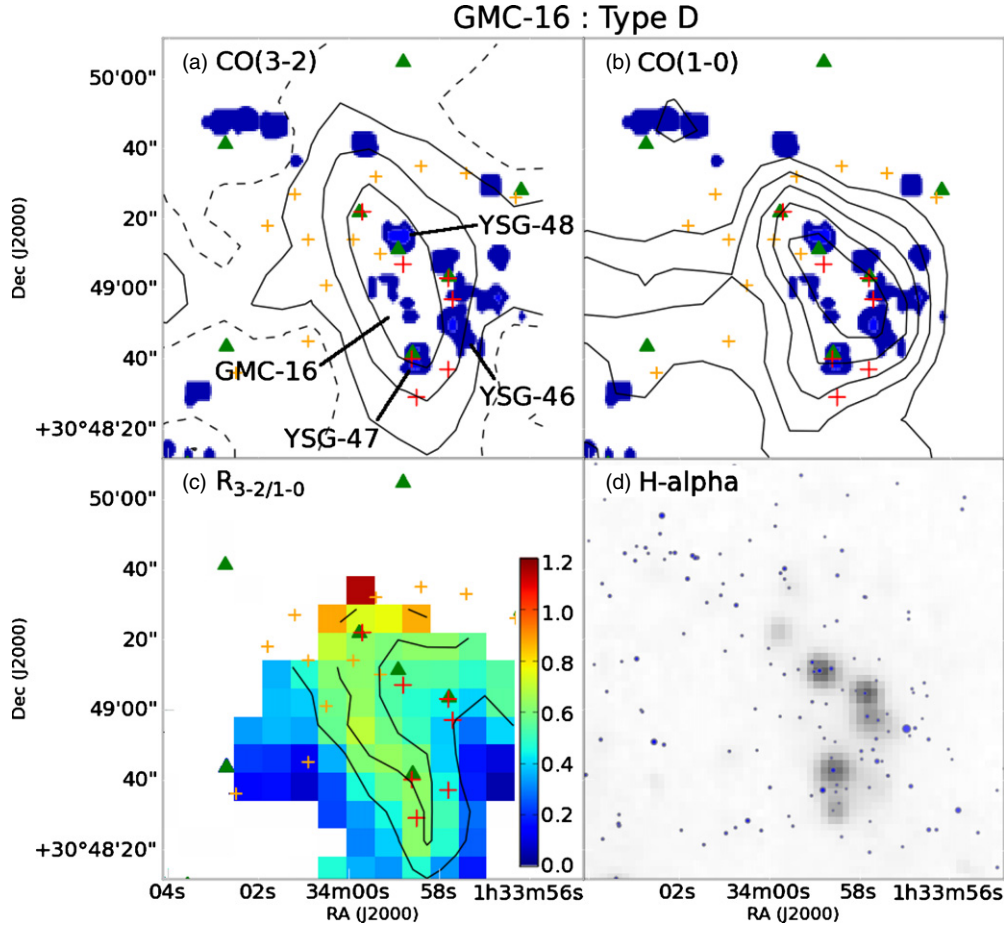


Figure 16. Same as Figure 13, but for GMC-16 representing Type D. The integrated velocity range used in the moment maps is $V_{\text{LSR}} = -264$ to -244 km s^{-1} .

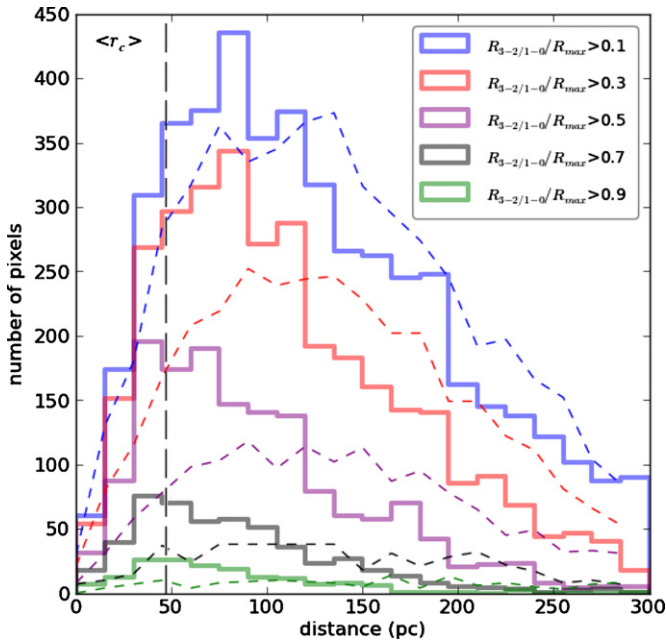


Figure 17. Frequency distribution of the projected distances from the nearest YSG of the pixels where $R_{3-2/1-0}$ is above 0.1 (blue line), 0.3 (red), 0.5 (purple), 0.7 (black), and 0.9 (green). For comparison, the dashed lines shows the frequency distribution of the distance when the YSGs are distributed randomly. The vertical (black) dashed line indicates the averaged size of the YSGs for reference.

5. SUMMARY

We present a GMC catalog using wide field (121 arcmin² in total) and high sensitivity ($1\sigma = 16\text{--}32 \text{ mK}$ in T_{mb} for a velocity resolution of 2.5 km s^{-1}) CO($J = 3\text{--}2$) maps of the nearby spiral galaxy M33 taken with the ASTE 10 m dish, and a complementary new catalog of YSGs for which we have estimated the ages.

We summarize our main results as follows.

1. We identify 71 CO($J = 3\text{--}2$) GMCs from the CO($J = 3\text{--}2$) data. We discard from the analysis six GMCs which are at the edges of the observed field. The remaining 65 GMCs are characterized by the deconvolved sizes in the range of 12–157 pc in radius and virial masses of $1.5 \times 10^4\text{--}8.9 \times 10^6 M_{\odot}$, which are comparable to those of GMCs in our Galaxy.
2. We identify 75 YSGs from the excess of the surface density map of young stars that are associated with the identified GMCs. The total number of O stars in a YSG spans from 9 to 169, corresponding to total stellar masses of $10^{3.5}\text{--}10^{4.7} M_{\odot}$, assuming that they have a Salpeter IMF. The YSG ages are also estimated using the Padova model, and are found to be in the range of 4–31 Myr (12 Myr on average). These values are comparable to those of typical OB associations.
3. We compare the GMCs with the distribution of YSGs and classical H II regions from a compilation in the literature. The identified 65 GMCs are successfully classified into four categories: Type A showing no sign of massive SF, Type B

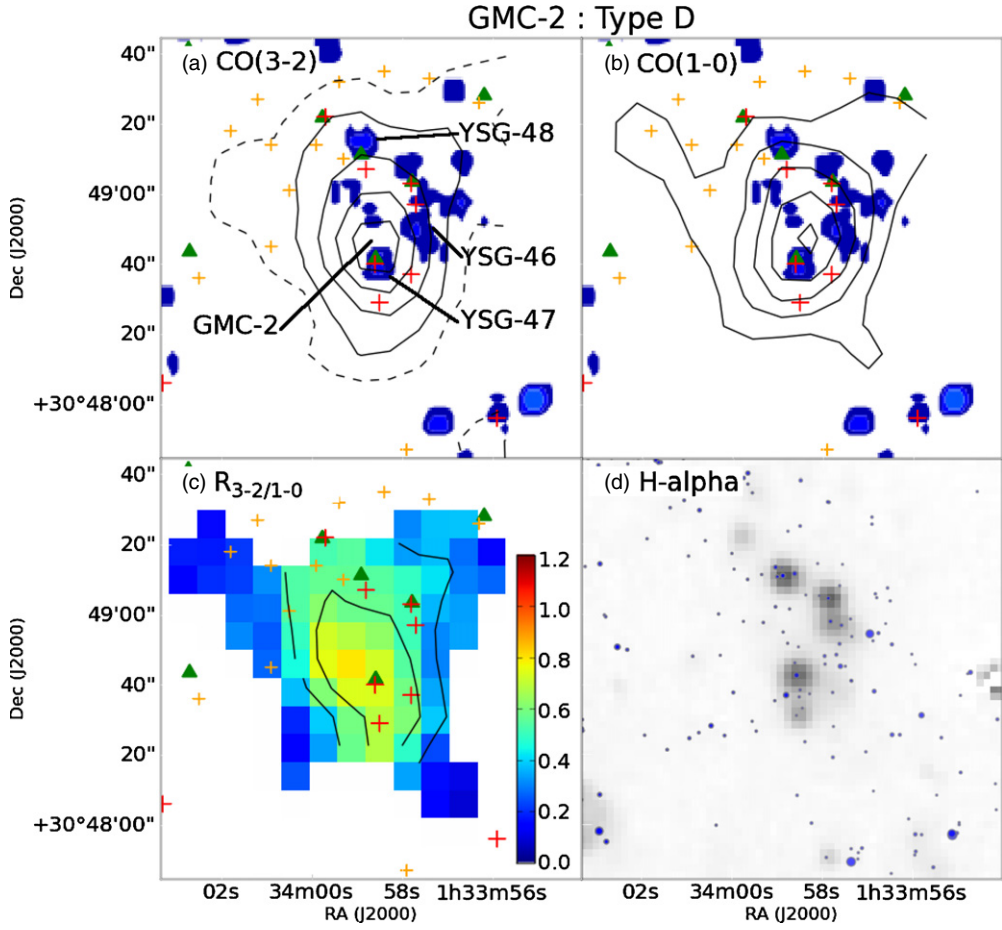


Figure 18. Same as Figure 13, but for GMC-2.

(A color version and the complete figure set (61 images) of this figure are available in the online journal.)

being associated only with relatively small H II regions, Type C with both H II regions and young (<10 Myr) stellar groups, and Type D with both H II regions and relatively old (10–30 Myr) stellar groups. Out of the 65 GMCs, 1 (1%), 13 (20%), 29 (45%), and 22 (34%) are found to be Types A, B, C, and D, respectively.

4. From a comparison of the distributions of the CO($J = 3-2$)/CO($J = 1-0$) intensity ratio, $R_{3-2/1-0}$, with the YSGs and H II regions, we find that the $R_{3-2/1-0}$ peaks within a GMC are slightly offset from the SF sites, but preferentially located around them.
5. We interpret the four types as representing an evolutionary sequence of the GMCs. Assuming that the number of the GMC types is proportional to the timescale of each evolutionary stage, we roughly estimate that they are ~ 1 , 3–7, 5–10, and 8–17 Myr, respectively for Types A, B, C, and D. This yields that the lifetime of a GMC with mass of $\gtrsim 10^5 M_\odot$ is 20–40 Myr, similar or slightly larger than the lifetime of LMC clouds.
6. Finally, we propose a scenario where after molecular gas becomes dense enough to form stars, massive SF occurs in such dense part. Then the molecular gas around the first-generation stars becomes dense and forms the new generation of stars. In this way, the SF propagates from the initially generated massive stars and continues during the GMC lifetime.

We thank the anonymous referee for a very useful report. We gratefully acknowledge the contributions of the ASTE staff to the development and operation of the telescope. The ASTE project is driven by Nobeyama Radio Observatory (NRO) and ALMA-J/Chile Observatory, branches of the National Astronomical Observatory of Japan (NAOJ), in collaboration with the University of Chile, and Japanese institutes including the University of Tokyo, Nagoya University, Osaka Prefecture University, Ibaraki University, Hokkaido University, Joetsu University of Education, Keio University, and Kyoto University. Observations with ASTE were in part carried out remotely from Japan by using NTT's GEMnet2 and its partner R&E (Research and Education) networks, which are based on AccessNova in a collaboration between the University of Chile, NTT Laboratories, and NAOJ.

Facilities: ASTE, No:45m

APPENDIX

SPATIAL COMPARISON OF GMCs, STELLAR GROUPS, AND H II REGIONS FOR INDIVIDUAL GMCs

Figure 18 (available in the online journal) shows the spatial comparison of GMCs, $R_{3-2/1-0}$, YSGs, and H II regions for the identified GMCs except those at the edge of the observed field, GMC-18, GMC-28, GMC-47, GMC-51, GMC-58 GMC-71, and also four GMCs that have been mentioned in Section 3.5.

REFERENCES

- Bastian, N., Ercolano, B., Gieles, M., et al. 2007, *MNRAS*, **379**, 1302
- Battinelli, P., Efremov, Y., & Magnier, E. A. 1996, *A&A*, **314**, 51
- Bica, E. L. D., & Schmitt, H. R. 1995, *ApJS*, **101**, 41
- Blitz, L. 1993, in *Protostars and Planets III*, ed. E. H. Levy & J. I. Lunine (Tucson, AZ: Univ. Arizona Press), 125
- Blitz, L., Fukui, Y., Kawamura, A., et al. 2007, in *Protostars and Planets V*, ed. B. Reipurth, D. Jewitt, & K. Keil (Tucson, AZ: Univ. Arizona Press), 81
- Boulesteix, J., Courtes, G., Laval, A., Monnet, G., & Petit, H. 1974, *A&A*, **37**, 33
- Bresolin, F. 2011, *ApJ*, **730**, 129
- Bruhweiler, F. C., Miskey, C. L., & Smith Neubig, M. 2003, *AJ*, **125**, 3082
- Calzetti, D., Kennicutt, R. C., Jr., Bianchi, L., et al. 2005, *ApJ*, **633**, 871
- Calzetti, D., Kennicutt, R. C., Engelbracht, C. W., et al. 2007, *ApJ*, **666**, 870
- Chandar, R., Bianchi, L., & Ford, H. C. 1999, *ApJ*, **517**, 668
- Churchwell, E., & Goss, W. M. 1999, *ApJ*, **514**, 188
- Corbelli, E., & Salucci, P. 2000, *MNRAS*, **311**, 441
- Courtes, G., Petit, H., Petit, M., Sivan, J.-P., & Dodonov, S. 1987, *A&A*, **174**, 28
- Drissen, L., Moffat, A. F. J., & Shara, M. M. 1990, *ApJ*, **364**, 496
- Drissen, L., Moffat, A. F. J., & Shara, M. M. 1993, *AJ*, **105**, 1400
- Emerson, D. T., & Graeve, R. 1988, *A&A*, **190**, 353
- Engargiola, G., Plambeck, R. L., Rosolowsky, E., & Blitz, L. 2003, *ApJS*, **149**, 343
- Ezawa, H., Kawabe, R., Kohno, K., & Yamamoto, S. 2004, *Proc. SPIE*, **5489**, 763
- Ezawa, H., Kohno, K., Kawabe, R., et al. 2008, *Proc. SPIE*, 7012, 701208
- Freedman, W. L., Madore, B. F., Gibson, B. K., et al. 2001, *ApJ*, **553**, 47
- Fukui, Y., & Kawamura, A. 2010, *ARA&A*, **48**, 547
- Fukui, Y., Kawamura, A., Minamidani, T., et al. 2008, *ApJS*, **178**, 56
- Fukui, Y., Mizuno, N., Yamaguchi, R., et al. 1999, *PASJ*, **51**, 745
- Girardi, L., Williams, B. F., Gilbert, K. M., et al. 2010, *ApJ*, **724**, 1030
- González Delgado, R. M., & Pérez, E. 2000, *MNRAS*, **317**, 64
- Gouliermis, D., Kontizas, M., Korakitis, R., et al. 2000, *AJ*, **119**, 1737
- Gouliermis, D. A., Schmeja, S., Klessen, R. S., de Blok, W. J. G., & Walter, F. 2010, *ApJ*, **725**, 1717
- Gratier, P., Braine, J., Rodriguez-Fernandez, N. J., et al. 2010, *A&A*, **522**, A3
- Gratier, P., Braine, J., Rodriguez-Fernandez, N. J., et al. 2012, *A&A*, **542**, A108
- Grossi, M., Corbelli, E., Giovanardi, C., & Magrini, L. 2010, *A&A*, **521**, A41
- Heyer, M. H., Corbelli, E., Schneider, S. E., & Young, J. S. 2004, *ApJ*, **602**, 723
- Hodge, P. W., Balsley, J., Wyder, T. K., & Skelton, B. P. 1999, *PASP*, **111**, 685
- Hoopes, C. G., & Walterbos, R. A. M. 2000, *ApJ*, **541**, 597
- Humphreys, R. M., & Sandage, A. 1980, *ApJS*, **44**, 319
- Hunter, D. A., Baum, W. A., O’Neil, E. J., Jr., & Lynds, R. 1996, *ApJ*, **456**, 174
- Hunter, D. A., Elmegreen, B. G., Dupuy, T. J., & Mortonson, M. 2003, *AJ*, **126**, 1836
- Hwang, N., & Lee, M. G. 2008, *AJ*, **135**, 1567
- Inoue, H., Muraoka, K., Sakai, T., et al. 2008, in *Proc. 19th Int. Symp. Space Terahertz Technology*, ed. W. Wild (Groningen: SRON), http://www.sron.nl/files/LEA/ISSTT2008/Proceedings_ISSTT2008.pdf, 281
- Ivanov, G. R. 2005, in *Proc. 4th Serbian–Bulgarian Astron. Conf.*, ed. M. S. Dimitrijević et al. (Belgrade: Publ. Astron. Soc. “Rudjer Bošković”), 75
- Ivanov, G. R., & Kunchev, P. Z. 1985, *Ap&SS*, **116**, 341
- Kaleida, C., & Scowen, P. A. 2010, *AJ*, **140**, 379
- Kawamura, A., Mizuno, Y., Minamidani, T., et al. 2009, *ApJS*, **184**, 1
- Kennicutt, R. C., Jr. 1989, *ApJ*, **344**, 685
- Kennicutt, R. C., Jr., Calzetti, D., Walter, F., et al. 2007, *ApJ*, **671**, 333
- Kennicutt, R. C., Jr., Hao, C.-N., Calzetti, D., et al. 2009, *ApJ*, **703**, 1672
- Kohno, K. 2005, in *ASP Conf. Ser. 344, The Cool Universe: Observing Cosmic Dawn*, ed. C. Lidman & D. Alloin (San Francisco, CA: ASP), 242
- Lada, C. J., & Lada, E. A. 2003, *ARA&A*, **41**, 57
- Liu, G., Koda, J., Calzetti, D., Fukuhara, M., & Momose, R. 2011, *ApJ*, **735**, 63
- Malumuth, E. M., Waller, W. H., & Parker, J. W. 1996, *AJ*, **111**, 1128
- Mangum, J. G., Emerson, D. T., & Greisen, E. W. 2007, *A&A*, **474**, 679
- Marigo, P., Girardi, L., Bressan, A., et al. 2008, *A&A*, **482**, 883
- Martins, F., Schaerer, D., & Hillier, D. J. 2005, *A&A*, **436**, 1049
- Massey, P. 2003, *ARA&A*, **41**, 15
- Massey, P., Olsen, K. A. G., Hodge, P. W., et al. 2006, *AJ*, **131**, 2478
- Massey, P., Olsen, K. A. G., Hodge, P. W., et al. 2007, *AJ*, **133**, 2393
- Mayya, Y. D., & Prabhu, T. P. 1996, *AJ*, **111**, 1252
- Minamidani, T., Mizuno, N., Mizuno, Y., et al. 2008, *ApJS*, **175**, 485
- Minamidani, T., Tanaka, T., Mizuno, Y., et al. 2011, *AJ*, **141**, 73
- Mizuno, N., Yamaguchi, R., Mizuno, A., et al. 2001, *PASJ*, **53**, 971
- Mizuno, Y., Kawamura, A., Onishi, T., et al. 2010, *PASJ*, **62**, 51
- Muraoka, K., Kohno, K., Tosaki, T., et al. 2007, *PASJ*, **59**, 43
- Muraoka, K., Tosaki, T., Miura, R., et al. 2012, *PASJ*, **64**, 3
- Onodera, S., Kuno, N., Tosaki, T., et al. 2010, *ApJ*, **722**, L127
- Onodera, S., et al. 2013, *PASJ*, in press
- Panagia, N., & Ranieri, M. 1973, *A&A*, **24**, 219
- Park, W.-K., & Lee, M. G. 2007, *AJ*, **134**, 2168
- Park, W.-K., Park, H. S., & Lee, M. G. 2009, *ApJ*, **700**, 103
- Pineda, J. L., Goldsmith, P. F., Chapman, N., et al. 2010, *ApJ*, **721**, 686
- Pineda, J. L., Mizuno, N., Stutzki, J., et al. 2008, *A&A*, **482**, 197
- Prescott, M. K. M., Kennicutt, R. C., Jr., Bendo, G. J., et al. 2007, *ApJ*, **668**, 182
- Rosolowsky, E., Keto, E., Matsushita, S., & Willner, S. P. 2007, *ApJ*, **661**, 830
- Rosolowsky, E., & Leroy, A. 2006, *PASP*, **118**, 590
- San Roman, I., Sarajedini, A., & Aparicio, A. 2010, *ApJ*, **720**, 1674
- San Roman, I., Sarajedini, A., Garnett, D. R., & Holtzman, J. A. 2009, *ApJ*, **699**, 839
- Sarajedini, A., & Mancone, C. L. 2007, *AJ*, **134**, 447
- Sault, R. J., Teuben, P. J., & Wright, M. C. H. 1995, in *ASP Conf. Ser. 77, Astronomical Data Analysis Software and Systems IV*, ed. R. A. Shaw, H. E. Payne, & J. J. E. Hayes (San Francisco, CA: ASP), 433
- Savage, B. D., & Mathis, J. S. 1979, *ARA&A*, **17**, 73
- Sawada, T., Ikeda, N., Sunada, K., et al. 2008, *PASJ*, **60**, 445
- Schlegel, D. J., Finkbeiner, D. P., & Davis, M. 1998, *ApJ*, **500**, 525
- Schmidt, M. 1959, *ApJ*, **129**, 243
- Sharma, S., Corbelli, E., Giovanardi, C., Hunt, L. K., & Palla, F. 2011, *A&A*, **534**, A96
- Solomon, P. M., Rivolo, A. R., Barrett, J., & Yahil, A. 1987, *ApJ*, **319**, 730
- Sorai, K., Sunada, K., Okumura, S. K., et al. 2000, *Proc. SPIE*, **4015**, 86
- Tosaki, T., Kuno, N., Onodera, S. M. R., et al. 2011, *PASJ*, **63**, 1171
- Tosaki, T., Miura, R., Sawada, T., et al. 2007, *ApJ*, **664**, L27
- Verley, S., Corbelli, E., Giovanardi, C., & Hunt, L. K. 2009, *A&A*, **493**, 453
- Verley, S., Corbelli, E., Giovanardi, C., & Hunt, L. K. 2010, *A&A*, **510**, A64
- Verley, S., Hunt, L. K., Corbelli, E., & Giovanardi, C. 2007, *A&A*, **476**, 1161
- Wilcots, E. M. 1994, *ApJ*, **108**, 1674
- Wilson, C. D., Walker, C. E., & Thornley, M. D. 1997, *ApJ*, **483**, 210
- Wilson, C. D., Warren, B. E., Israel, F. P., et al. 2009, *ApJ*, **693**, 1736
- Wyder, T. K., Hodge, P. W., & Skelton, B. P. 1997, *PASP*, **109**, 927
- Yamaguchi, R., Mizuno, N., Mizuno, A., et al. 2001, *PASJ*, **53**, 985